Cretaceous continental margin evolution revealed using quantitative seismic geomorphology, offshore northwest Africa

Max Casson, Gérome Calves, Mads Huuse, Ben Sayers, Jonathan Redfern

Received: 27 September 2019 | Revised: 31 March 2020 | Accepted: 2 April 2020

DOI: 10.1111/bre.12455

ORIGINAL ARTICLE

Basin Research | IAS EAGE | WILEY

Cretaceous continental margin evolution revealed using quantitative seismic geomorphology, offshore northwest Africa

Max Casson[1] | **Gérôme Calvès**[2] | **Mads Huuse**[1] | **Ben Sayers**[3] | **Jonathan Redfern**[1]

[1]North Africa Research Group (NARG), Department of Earth and Environmental Sciences, The University of Manchester, Manchester, UK

[2]Faculté sciences et ingénierie, Université Toulouse 3 - Paul Sabatier, Toulouse, 31062, France

[3]TGS, Surrey, UK

Correspondence
Max Casson, North Africa Research Group (NARG), Department of Earth and Environmental Sciences, The University of Manchester, Williamson Building, Oxford Road, Manchester M13 9PL, UK.
Email: max.casson@manchester.ac.uk

Abstract

The application of high-resolution seismic geomorphology, integrated with lithological data from the continental margin offshore The Gambia, northwest Africa, documents a complex tectono-stratigraphic history through the Cretaceous. This reveals the spatial-temporal evolution of submarine canyons by quantifying the related basin depositional elements and providing an estimate of intra- versus extra-basinal sediment budget. The margin developed from the Jurassic to Aptian as a carbonate escarpment. Followed by, an Albian-aged wave-dominated delta system that prograded to the palaeo-shelf edge. This is the first major delivery of siliciclastic sediment into the basin during the evolution of the continental margin, with increased sediment input linked to exhumation events of the hinterland. Subaqueous channel systems (up to 320 m wide) meandered through the pro-delta region reaching the palaeo-shelf edge, where it is postulated they initiated early submarine canyonisation of the margin. The canyonisation was long-lived (*ca*. 28 Myr) dissecting the inherited seascape topography. Thirteen submarine canyons can be mapped, associated with a Late Cretaceous-aged regional composite unconformity (RCU), classified as shelf incised or slope confined. Major knickpoints within the canyons and the sharp inflection point along the margin are controlled by the lithological contrast between carbonate and siliciclastic subcrop lithologies. Analysis of the base-of-slope deposits at the terminus of the canyons identifies two end-member lobe styles, debris-rich and debris-poor, reflecting the amount of carbonate detritus eroded and redeposited from the escarpment margin (blocks up to *ca*. 1 km^3). The vast majority of canyon-derived sediment (97%) in the base-of-slope is interpreted as locally derived intra-basinal material. The average volume of sediment bypassed through shelf-incised canyons is an order of magnitude higher than the slope-confined systems. These results document a complex mixed-margin evolution, with seascape evolution, sedimentation style and volume controlled by shelf-margin collapse, far-field tectonic activity and the effects of hinterland rejuvenation of the siliciclastic source.

KEYWORDS

Central Atlantic, continental margin sedimentary processes, mixed siliciclastic–carbonate systems, quantitative seismic geomorphology, regional composite unconformity, submarine canyons

1 | INTRODUCTION

Continental margins through the rift to drift stages of the Wilson cycle are major archives of the stratigraphic record (Bond & Kominz, 1988; Bradley, 2008). Following a period of initial extension induced by rifting processes (McKenzie, 1978), continental breakup and related oceanic crust formation (rift to drift transition) is typically marked by a break-up unconformity (Braun & Beaumont, 1989). Younger post-rift stratigraphy traditionally 'passively' infills the accommodation generated by thermal subsidence of the margin (Bond, Kominz, Steckler, Grotzinger, & Crevello, 1989; Steckler, Watts, & Thorne, 1988). The fill of these basins host 35% of known giant hydrocarbon discoveries (Mann, Gahagan, & Gordon, 2003). These extensive basins have been evaluated in deep-sea boreholes, hydrocarbon exploration wells, exhumed outcrops, seafloor geophysical and seismic reflection data. Since the first recognition of 'Atlantic-type' margins by Suess in 1885 (Bond & Kominz, 1988), findings from these datasets have been used to pioneer our understanding of continental margins and to develop fundamental knowledge of earth system processes, i.e. continental drift (Wegener, 1912). New techniques, i.e. seismic stratigraphy (Mitchum & Vail, 1977), seismic geomorphology (Posamentier & Kolla, 2003) and source-to-sink analysis (Allen, 2008; Clift et al., 2008; Martinsen, Sømme, Thurmond, Helland-Hansen, & Lunt, 2010; Sømme, Helland-Hansen, Martinsen, & Thurmond, 2009), have been used to investigate continental margin sedimentary systems. These observations document the stratigraphic record to calibrate studies modelling the solid earth (Burgess, 2001; Granjeon & Joseph, 1999; Moucha et al., 2008).

Study of continental margin sedimentary systems has remained conventionally divided into siliciclastic and carbonate realms (Chiarella, Longhitano, & Tropeano, 2017). Moscardelli, Ochoa, Lunt, and Zahm (2019) highlighted the apparent lack of complete examples using modern data to document mixed siliciclastic–carbonate systems in the literature. Mixed siliciclastic–carbonate systems or 'mixed systems' are defined by contemporaneous siliciclastic and carbonate sedimentation in the stratigraphic record. Mixing occurs across the full length of the depositional system. Shallow marine to shelf settings exhibit a complex interaction between fluvio-deltaic and shallow marine siliciclastic systems with intervening carbonate factories (e.g. Chiarella & Longhitano, 2012). Deep-water settings are significantly different, here mixing occurs when siliciclastic and carbonate sediment is redeposited by a range of sedimentary gravity flow types (e.g. Payros & Pujalte, 2008; Playton, Janson, Kerans, James, & Dalrymple, 2010).

The continental margins of the Central Atlantic developed as mixed systems during the Cretaceous, subsequently deeply dissected by submarine canyon systems (Meyer, 1989; Mourlot, Calvès, et al., 2018; Mourlot, Roddaz, et al., 2018). Canyons on continental margins act as key pathways for sediment transported from the shelf to deep basin (Davies, Roberts, & Hall-Spencer, 2007; Fildani, 2017; Harris & Whiteway, 2011; Normark, 1974; Normark & Piper, 1969). The seascape geomorphology is deeply shaped by these long-lived systems (Pratson et al., 2007). Within this complex depositional and erosional template, fundamental sedimentary processes persist and carve the morphology of continental margins: sedimentary gravity flows and mass wasting events (gravitational processes), modified by along-slope oceanographic currents.

This study examines a high-resolution three-dimensional (3D) seismic dataset offshore The Gambia, northwest Africa to study continental margin evolution, while examining the style and evolution of buried submarine canyons with associated base-of-slope deposits (Figure 1). The study area is located in an important position within the source-to-sink system, covering the shelf, through the slope to the basin floor (Martinsen et al., 2010). Quantitative seismic geomorphology techniques are used (Posamentier & Kolla, 2003; Wood, 2007), integrated with exploration and scientific well data to reconstruct sedimentary processes and margin morphology over million-year geological timescales (Figure 2; Pratson et al., 2007).

2 | REGIONAL SETTING

The conjugate continental margins of northwest Africa and Eastern America developed following the formation of the Central Atlantic in the early Mesozoic (Davison, 2005; Labails, Olivet, Aslanian, & Roest, 2010; Uchupi & Emery, 1991; Uchupi, Emery, Bowin, & Phillips, 1976). The stratigraphy along the northwest African Atlantic Margin (NWAAM) records rifting in the Late Triassic (Davison, 2005); opening of the Central Atlantic in the Middle Jurassic (Labails, 2007) and thermal subsidence in the Jurassic to Recent (Latil-Brun & Lucazeau, 1988), from northern Morocco to the Guinea Fracture Zone. The study area is located at the northernmost tip of the Casamance sub-basin (Figure 1a). The margin is structurally segmented by Pan-African structures and later transform faults (Brownfield & Charpentier, 2003). The sub-basin contains allochthonous salt that is remobilised (Tari, Molnar, & Ashton, 2003). The study area is located outboard of the Casamance failed rift arm, which is postulated to have controlled the antecedent drainage of the proto-Gambia river (Figure 1; Long & Cameron, 2016).

The Mesozoic post-rift evolution of the basin fill initiated with the establishment of an extensive Tethyan-type carbonate platform surrounding the Central Atlantic margins. During the Albian, the platform died out as siliciclastic sedimentation proceeded to dominate (Martin, Effimoff,

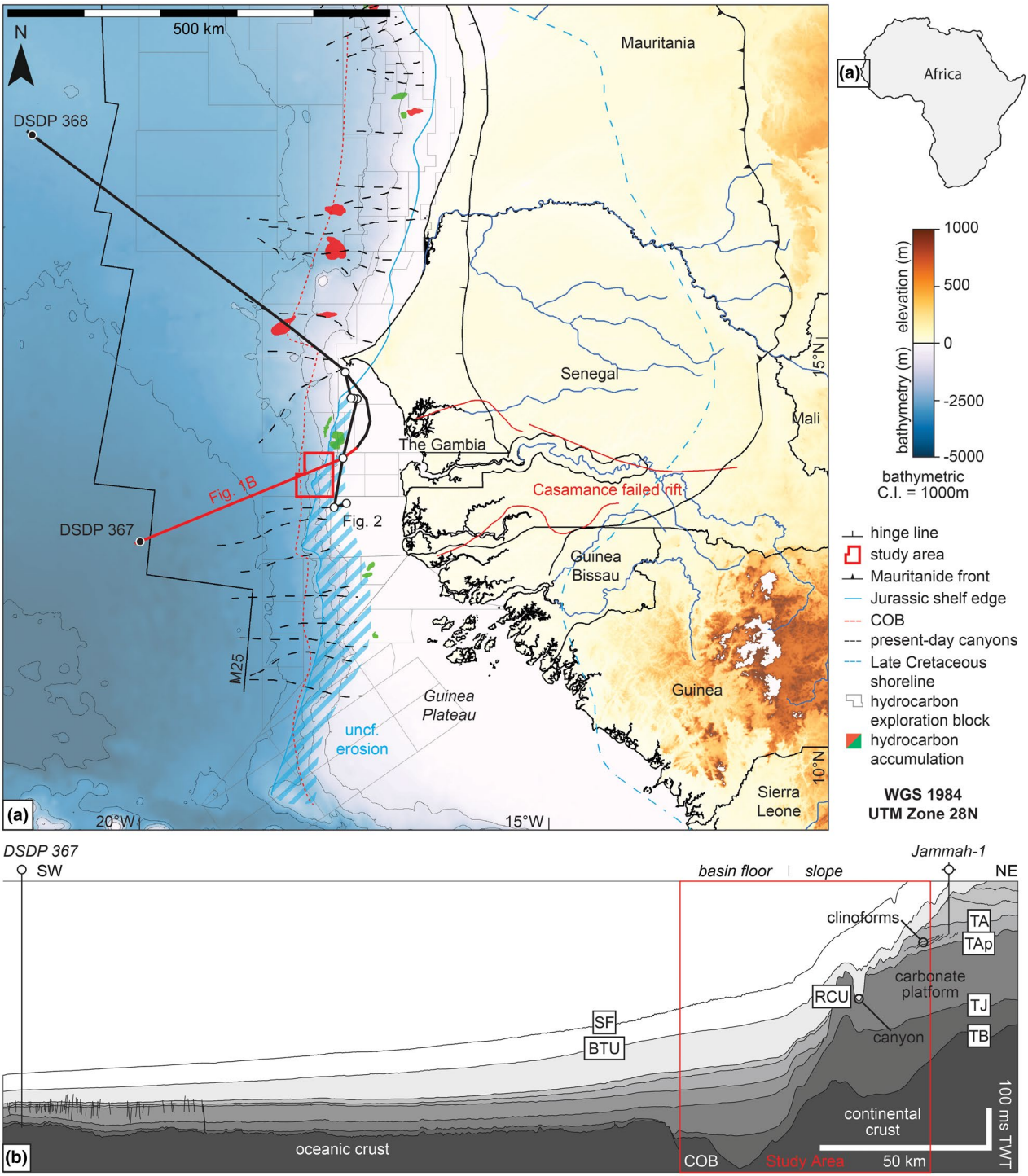

FIGURE 1 (a) Shaded bathymetric and topographic map of northwest Africa showing the present-day structure of the continental margin, with major river systems delineated (blue lines). The M25 (154 Ma) magnetic anomaly is shown as a black line and the continent–ocean boundary (COB) as a red dashed line after Labails et al. (2010). The 3D seismic reflection dataset in hydrocarbon exploration blocks A1 and A4, offshore The Gambia (WGS 1984 UTM Zone 28N) is tied to Deep Sea Drilling Project (DSDP) sites 367 and 368 by regional 2D seismic reflection data. The study area covers the present-day shelf-to-basin transition. The location of the well correlation in Figure 2 is shown; see Figure 2 inset for a more detailed map naming the exploration wells. Hydrocarbon accumulations along the margin are displayed. The eastern margin of the Mauritania–Senegal–Guinea–Bissau–Conakry (MSGBC) Basin is defined by the Mauritanide front (Labails et al., 2010). The Mesozoic shelf edge (after Purdy, 1989), Late Cretaceous shoreline and erosion (after Mourlot, Calvès, et al., 2018; Mourlot, Roddaz, et al., 2018), and Casamance failed rift arm (after Long, 2016) are mapped. Present-day canyon systems locations from Wynn (2000a). (b) Regional cross section based on the 2D seismic line. See (A) for location. BTU, Base Tertiary Unconformity; RCU, Regional Composite Unconformity; SF, Seafloor; TA, Top Albian; TAp, Top Aptian; TB, Top Basement; TJ, Top Jurassic

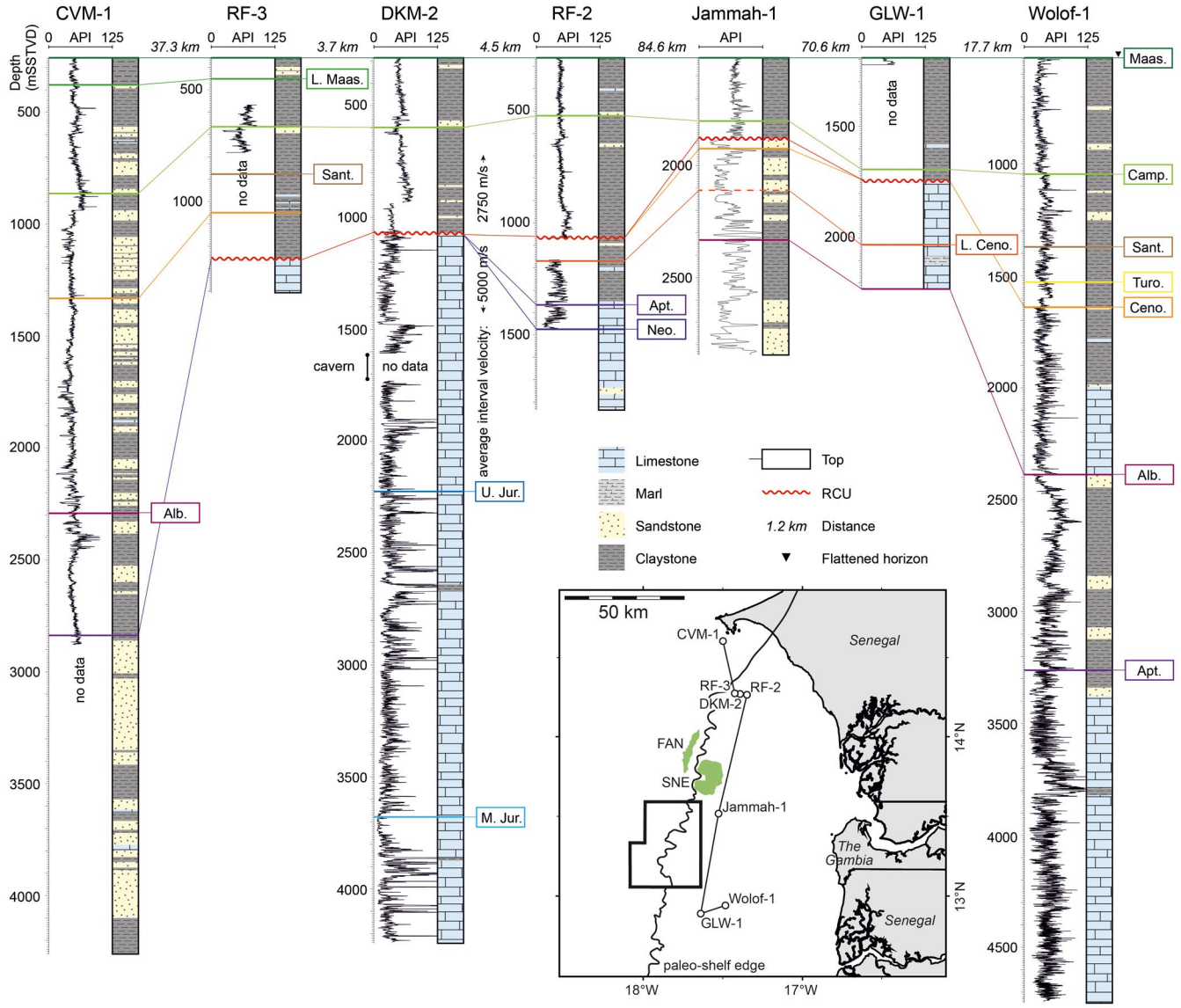

FIGURE 2 Senegal-Gambia stratigraphy. Regional well correlation, datum the base Tertiary unconformity, along a 200-km strike profile of the NWAAM. Biostratigraphy and formation tops evaluated from well reports. Average interval velocities (m/s) above and below the regional composite unconformity are displayed. Data courtesy of Petrosen. Jammah-1 data from Clayburn (2017). Inset maps shows location of the wells, study area, palaeo-shelf edge and hydrocarbon discoveries (green)

Medou, & Laughland, 2010). At this time, the opening of the Equatorial Atlantic gateway influenced palaeo-circulation in the Central Atlantic (Förster, 1978) influencing the depositional systems in the deep basin (Mourlot, Calvès, et al., 2018; Mourlot, Roddaz, et al., 2018) and a transpressional tectonic regime was established along the southern NWAAM and conjugate Demerara Plateau (Reuber, Pindell, & Horn, 2016). Subsequently, Albian deltas prograded across the platform, forming the prolific pro-delta hydrocarbon reservoirs of the SNE field, Senegal (Clayburn, 2017). The Cenomanian transgression and the altered circulation patterns associated with the opening of the Equatorial Atlantic formed a coastal upwelling zone of deeper oceanic water masses off the NWAAM (Arthur, Dean, & Stow, 1984). This resulted in the deposition of *ca*. 150-m-thick organic-rich interval (av. TOC—10%; Arthur et al., 1984) on the basin floor (encountered at DSDP Site 367) onlapping onto the wide transgressed shelf and coastal basin.

The Santonian compressional event (84–80 Ma) associated with Africa–Europe convergence caused inversion of sedimentary basins in North Africa and at this time there was also a change in the pole of rotation in the opening Central Atlantic (Labails, 2007). Regional uplift of the NWAAM accompanied these tectonic events, manifesting as a Late Cretaceous regional composite unconformity (RCU) that can be recognised along the entirety of the margin south of Dakar (*ca*. 660 km; Figure 1). This feature has previously been termed the Senonian unconformity

(Tari et al., 2003) and pre-Maastrichtian unconformity (Clayburn, 2017). The tectonism coincided with relatively high sea level and a transgressed onshore basin during the Late Cretaceous greenhouse period (Figure 1; Haq, 2014). Destabilisation of the distal continental margin resulted in margin collapse, with erosion focused at the palaeo-shelf edge removing up to 1.5 km of sediment (Figure 1; Mourlot, Calvès, et al., 2018; Mourlot, Roddaz, et al., 2018; Tari et al., 2003). The margin remains heavily canyonised to present day (Figure 1; Wynn, Masson, Stow, & Weaver, 2000a). It is postulated that, despite the high sea level, uplift was such that the platform was subaerially exposed at this time, resulting in karstification (Martin et al., 2010; Tari et al., 2003). A major Cenozoic magmatic event affected the area surrounding Dakar, Senegal (Goumbo Lo, Dia, & Kampunzu, 1992).

Historically, the American margin has been a key region for the study of submarine canyons (Dugan & Flemings, 2000; Fulthorpe, Austin, & Mountain, 2000; McHugh, Ryan, & Schreiber, 1993; Mitchell, 2005; Miller, Melillo, Mountain, Farre, & Wylie Poag, 1987). Comparatively less work has documented the African conjugate (Antobreh & Krastel, 2006). However, there is now increased interest as recent significant hydrocarbon accumulations (e.g. SNE field, Senegal—Clayburn, 2017) indicate submarine canyons here are an important palaeogeomorphic trapping mechanism for oil and gas. They also spatially control delivery of reservoir sands into the deep basin (e.g. Greater Tortue Ahmeyim field, Mauritania-Senegal—Kosmos Energy, 2017), and their fill may form attractive hydrocarbon exploration targets.

3 | DATASET and METHODS

3.1 | Data

The subsurface dataset offshore The Gambia consists of a 3D seismic reflection survey covering exploration blocks A1 and A4, and one regional 2-D seismic tie line linking the 3D survey to DSDP sites 367 and 368 (VER01 MWT). The 3D seismic survey covers an area of 2,566 km^2 across the present-day mid-to-lower slope, with water depths ranging from 279 to 3,524 m. Across all surveys, the seismic data are presented in zero phase and follows SEG normal polarity convention: where a downward increase in acoustic impedance is represented by a peak (black) reflection event, and a trough (red) event is associated with the opposite downward impedance decrease. The bin spacing is 12.5 × 25 m. In the interval of interest (3–6.5 s TWT), the dominant frequency is around 35 Hz. Using an average velocity of 2,750 m/s for the overlying Late Cretaceous to Recent sediments (based on well DKM-2: Figure 2), and the vertical resolution (λ/4) is *ca.* 20 m. Additionally, wireline data and final well reports from six exploration wells drilled offshore Senegal are correlated along a 200 km strike profile of the NWAAM (Figure 2; data provided by Petrosen). The gamma ray log and lithological data for well Jammah-1 offshore The Gambia was published by Clayburn (2017).

3.2 | Methods

Seismic interpretation of key horizons was performed using the methods of Posamentier (2005; Figure 3). Age constraints for the key stratigraphic surfaces were attained from nearby exploration wells and correlated with the 3D seismic dataset using the 2D regional tie line. The stratigraphy and age model in the DSDP boreholes have been recently re-evaluated (Mourlot, Calvès, et al., 2018; Mourlot, Roddaz, et al., 2018). Using the available well data, we have established a correlation between key horizons on the platform, across the escarpment margin, into the basin.

The RCU (Figure 4) was manually interpreted and converted into depth using a simple average interval velocity model (data extrapolated from well DKM-2). We recognise uncertainty is inherent in the depth conversion process, however, this provides more accurate geometries than a time structure map and was the best depth conversion method available. The surface was 'restored' to the depositional geometry by flattening on the top Aptian horizon (Figure 4). We interpret this horizon to have been a relatively flat depositional surface at the scale of the study area (horizontal extent of flattened surface and carbonate platform is 7.5–30 km; Figure 6a). This flattened topography is recognised on comparable distal carbonate platforms (Kenter & Campbell, 1991). Major structural and tectonic modification of this surface occurred following canyon incision. The depth-converted surface was exported to ESRI ArcMap v. 10.4.1 and the Arc Hydro module used to calculate drainage catchments and subsequently flow pathways. This workflow is commonly used in hydrology to simulate drainage patterns of rivers (Maidment & Morehouse, 2002), and to extract modern-day submarine drainage (i.e. California margin; Pratson & Ryan, 1996). Flow pathways recording submarine canyons are labelled from North to South, A1 to M (Figure 4a). From the RCU horizon, there was further extraction of quantitative seismic geomorphological data to characterise the submarine canyons (Figure 3).

The top Aptian and base Tertiary unconformity were initially interpreted manually. These key surfaces and the RCU were used to constrain a geo-model in PaleoScan™. Semi-automated seismic interpretation in PaleoScan™ produced a 200-horizon stack of stratigraphically concordant slices with extracted seismic attributes such as RMS amplitude (Figure 8) and variance. GeoTeric software was used to perform spectral decomposition by extracting an amplitude spectrum and

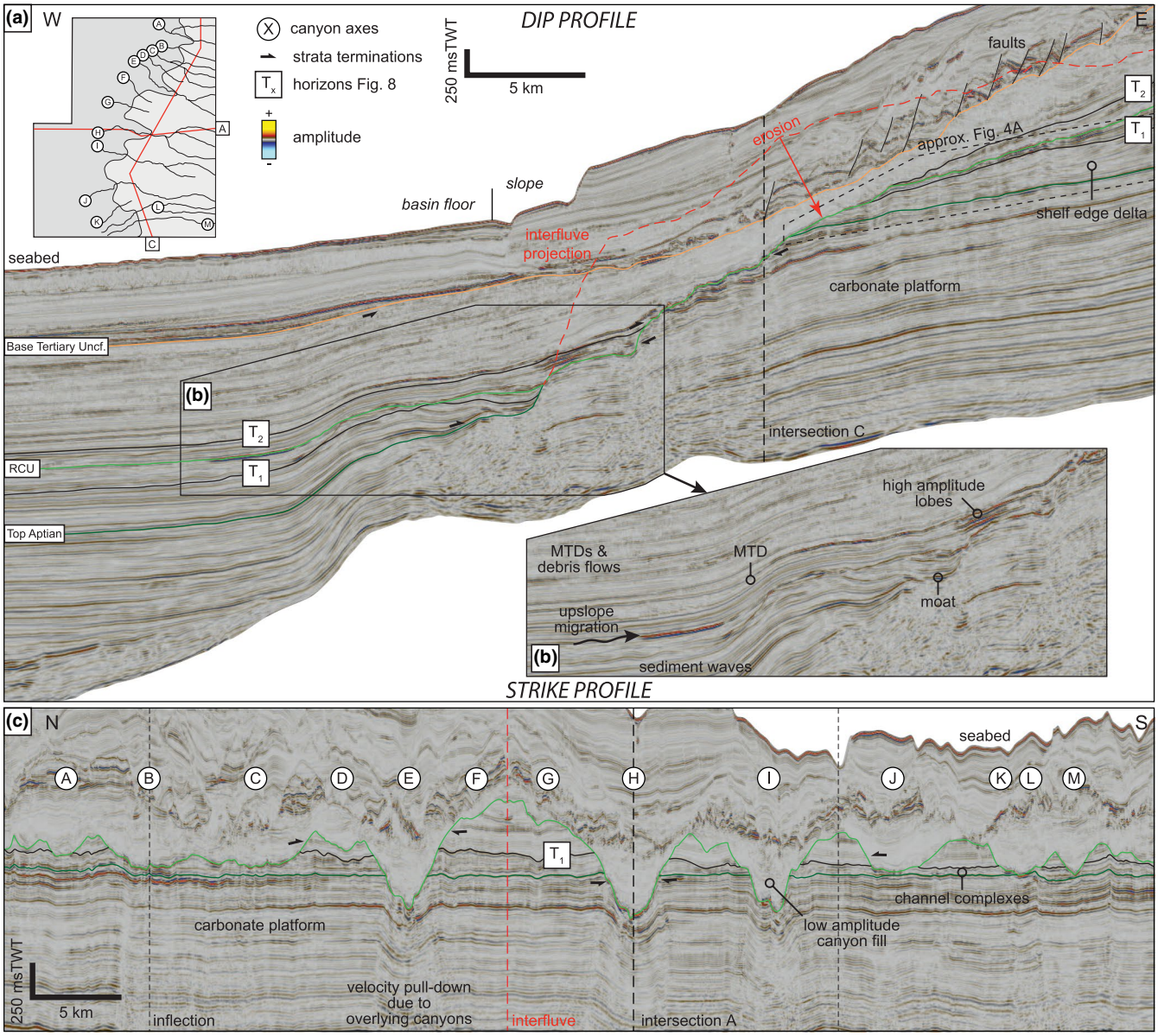

FIGURE 3 (a) East-West two-way time seismic section with interpreted key stratigraphic surfaces. The regional composite unconformity (RCU) surface on the adjacent interfluve is projected onto the dip profile (dashed red line) highlighting the amount of erosion in canyon H. Intersections shown in (c). (b) Inset seismic section focusing on seismic facies identified at the base of the canyon, MTD, mass transport deposit. (c) North–South two-way time seismic section with canyon axes displayed. See inset map (a) for the line locations. Seismic data courtesy of TGS

assigning each frequency bin, 20–30–40 Hz, with the colours red, green and blue respectively. These volumes were blended to produce the spectral decomposition images (Figure 7). Integration of the data from these seismic attributes and acoustic characteristics was used to identify seismic facies characteristic of deep-water architectural elements (canyons, channels, lobes, mass transport deposits/MTDs and sediment waves) after Posamentier and Kolla (2003). These features are associated with specific canyons and plotted against relative time (horizon 1–200) from the PaleoScan™ model to understand the spatial and temporal evolution of the depositional systems. A Geobody interpretation in PaleoScan™ was performed to extract quantitative data for the basin deposits (Table 1).

4 | RESULTS

4.1 | Lithological & stratigraphic control

The following description of the lithologies and a regional stratigraphic correlation is provided to establish a framework for the detailed seismic interpretation (Figure 2). The Jurassic to Aptian stratigraphy, as encountered in wells RF-3, DKM-2, RF-2 and Wolof-1, penetrated a thick succession of carbonate lithologies (up to 3,100 m thick in well DKM-2; Figure 2). These generally consist of interbedded micritic limestones, rare oolitic, sucrosic secondary dolomite, cemented calcareous sandstones and occasional

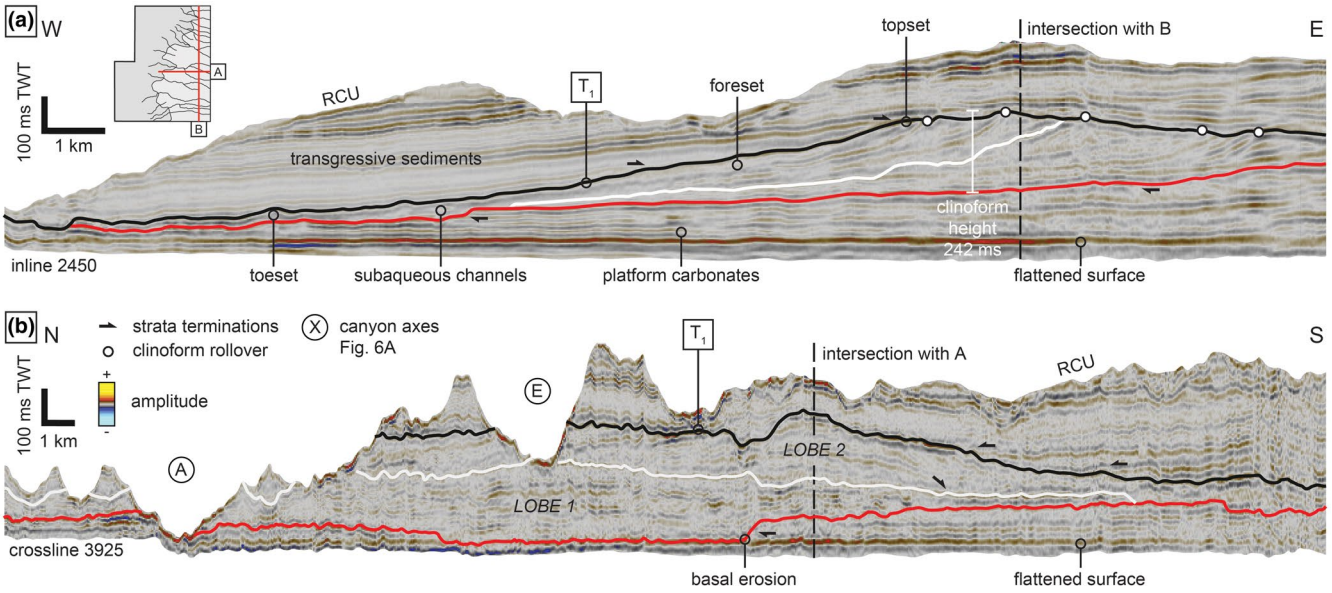

FIGURE 4 (a) Interpreted dip two-way time seismic section of the progradational shelf-edge delta shown in Figure 3a. Section flattened on the top Aptian surface shown in Figure 3a to 'restore' the depositional geometry. (b) Interpreted strike two-way time seismic section. Only seismic data between the regional composite unconformity (RCU) and −20 ms TWT below the top Aptian are shown. See inset map (a) and Figure 5c for the line locations. Seismic data courtesy of TGS

interbedded mudstones. These heterogeneous strata characterise the deposits of the carbonate platform. Outboard of the platform, well CVM-1 records an Aptian basin stratigraphy that is predominantly composed of mixed lithologies; comprising cemented very fine-grained sandstones to sandy micritic limestones, interbedded with mudstones. At DSDP Site 367 (Core 25–32; Lancelot et al., 1978a; Figure 1b) and also exposed on Maio, Cape Verde islands (Casson, Bulot, Jeremiah, & Redfern, 2020), the time-equivalent distal stratigraphy of the carbonate platform is composed of thin-bedded pelagic limestone interbedded with marls and black shale.

Overlying the carbonate platform, the Albian sequence, as penetrated in the inboard wells, Jammah-1 and Wolof-1, is principally mudstone dominated with thick units of very fine-grained sandstone. Regionally, the siliciclastic Albian strata form hydrocarbon reservoirs in the SNE and FAN discoveries deposited within a pro-delta apron and as basin-floor contourites respectively (Figure 2; Clayburn et al., 2017). This corresponds to a major lithological transition from carbonate- to siliciclastic-dominated stratigraphy recorded across most of the Central Atlantic in the oceanic domain (Casson et al., 2020). Where present, the Cenomanian–Turonian interval is characterised by heterogeneous assemblage of thin sandstones and limestones within a highly organic shale-prone interval. TOC values vary in the shales attaining up to 36% at DSDP Site 367 (Lancelot et al., 1978a, 1978b), and decrease onto the shelf (Arthur et al., 1984). Overlying this, the Coniacian to Maastrichtian interval is a thick succession of non-calcareous silty shale, with an upward increase in sandy shale beds and sandstone inter-beds.

We interpret the top of the main Jurassic to Lower Cretaceous carbonate platform to be approximately the top Aptian marker. Locally in well Wolof-1, there is evidence for sandstone deposition during the Aptian, and in well GLW-1, the Cenomanian interval is limestone dominated (Figure 2). This variable spatial and temporal distribution of carbonate is to be expected on a mixed-system margin where carbonate factories exist in areas along strike where siliciclastic sediment input is absent or limited (i.e. Moscardelli et al., 2019).

The RCU is observed in five of the seven wells studied, variably eroding into the underlying stratigraphy (Figures 2 and 6). Erosion is generally greatest in proximity to the palaeo-shelf edge, as indicated by well DKM-2, where the RCU erodes deeply into the Lower Cretaceous carbonate platform. Further inboard, in well Wolof-1, a more expanded Aptian and younger stratigraphy is preserved. Outboard of the platform edge, there is no clear record of the RCU in well CVM-1 where Coniacian- to Maastrichtian-aged sediments overlie the RCU.

Palaeo-water depth indicators from foraminiferal analysis of sediments recovered from well GLW-1, located on the shelf, indicate a deepening in palaeo-water depth across the RCU from shallow marine to deep water slope settings. Seismic evidence (i.e. the first record of canyon-related basin deposits) suggests the onset of canyon formation and hence establishment of the RCU occurred in the early Late Cretaceous.

TABLE 1 Geomorphological data extracted from the sediment flow pathways (Arc Hydro) and regional composite unconformity (RCU) surface. Shelf-un, shelf-incising ungraded canyons; shelf-gr, shelf-incising graded canyons; slope, slope-confined canyons. Bold values signify the sediment flow pathway extended beyond the study area

Canyon ID	Type	Total length (m)	Straight length (m)	Sinuosity	Max. width (m)	Max. incision (m)	Distance eroded (m)	Mean Azimuth
A1	Shelf-un	17,128	14,632	1.2	2,172		**7,239**	274.2
A2	Shelf-un	12,273	11,862	1.0	3,718	679	**5,125**	283.8
B	Shelf-un	16,059	15,668	1.0	3,845	102	**10,752**	285.2
C1	Shelf-un	17,908	17,104	1.0	2095		**9,836**	285.0
C2	Shelf-un	12,703	12,307	1.0	1645		**7,863**	289.5
C3	Shelf-un	11,144	9,508	1.2	2,328	534	**12,867**	301.5
D	Slope	12,075	11,133	1.1	2,134	212	4,289	305.1
E1	Shelf-gr	25,439	21,380	1.2	2,741		**10,892**	292.6
E2	Shelf-gr	8,051	7,980	1.0	6,308	3,976	**13,086**	300.4
F	Slope	10,534	9,999	1.1	2023	199	3,896	312.3
G	Slope	11,287	10,949	1.0	2,493	298	3,920	283.5
H1	Shelf-gr	32,979	30,348	1.1	1657		**17,640**	269.7
H2	Shelf-gr	11,198	10,930	1.0	1970		**18,463**	289.8
H3	Shelf-gr	15,799	14,284	1.1	7,030	3,561	**19,735**	294.4
I1	Shelf-un	33,836	31,385	1.1	2050		**22,947**	283.8
I2	Shelf-un	8,630	8,205	1.1	6,138	1974	16,872	289.0
J	Shelf-un	38,158	33,626	1.1	5,073	1568	**28,462**	270.3
K	Slope	11,565	10,760	1.1	1519	319	1,296	238.8
L1	Shelf-un	32,915	30,172	1.1	3,942		**21,058**	257.7
L2	Shelf-un	16,603	15,150	1.1	1782	936	**23,985**	279.1
M	Shelf-un	29,658	28,057	1.1	2,235	1,297	**19,475**	263.6
Mean	Shelf-un	20,585	18,973		3,085	1,013	15,540	
	Shelf-gr	18,693	16,984		3,941	3,769	15,963	
	Slope	11,365	10,710		2042	257	3,350	
	Total	18,378	16,926		3,090	1,204	13,319	

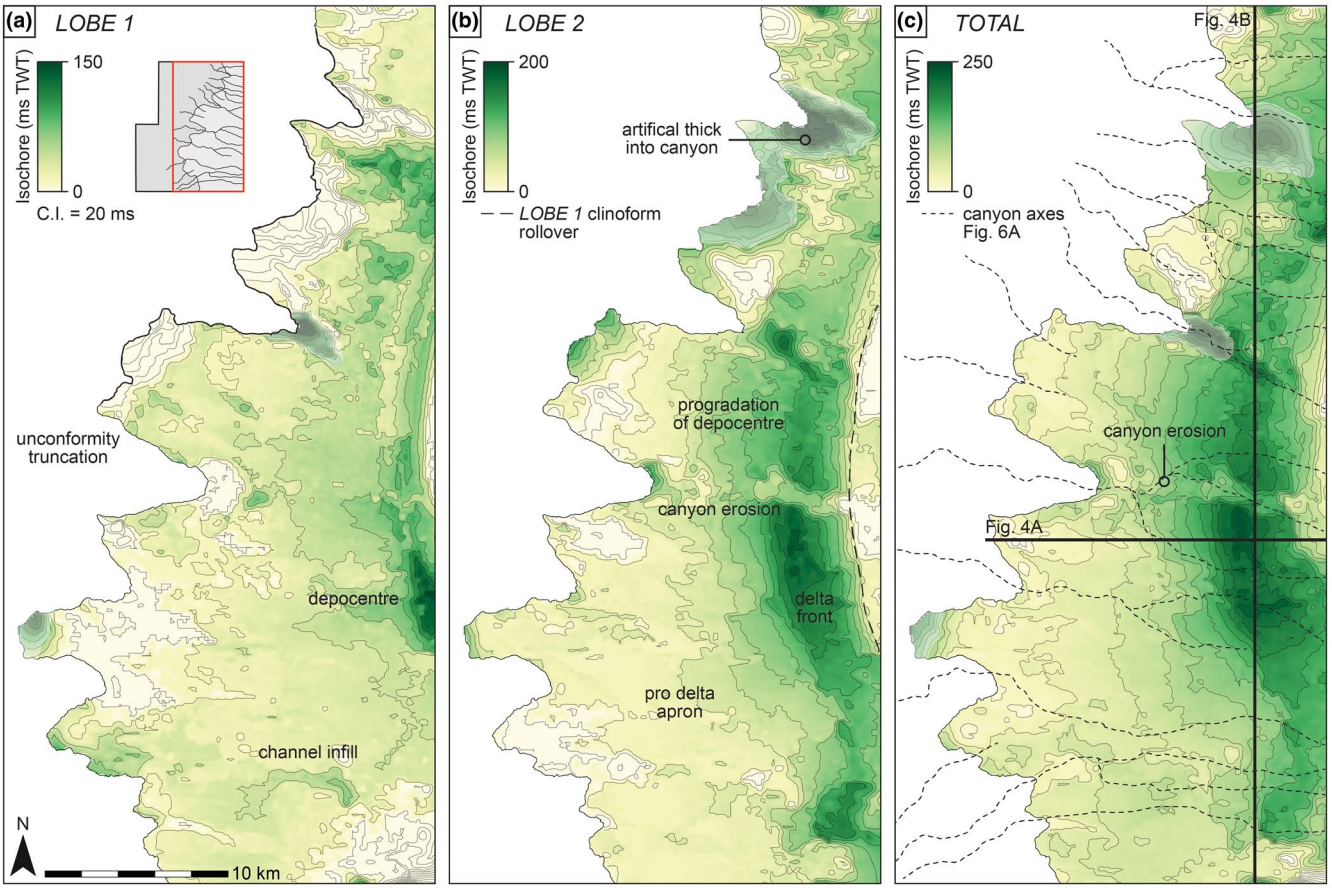

FIGURE 5 Isochore maps (ms TWT) showing the progradation of an Albian-aged shelf-edge delta system across the platform, truncated by RCU erosion at the carbonate escarpment margin. (a) Isochore map of Lobe 1. See inset map for location of displays in the study area (red box). (b) Isochore map of Lobe 2 highlighting the progradation of the system. (c) Total isochore for the shelf-edge delta. See Figure 4 for the seismic horizons mapped for lobes 1 and 2

4.2 | Margin structure

The large-scale stratal architecture of The Gambian continental margin is very well imaged on the 3D seismic and characterised as a relict carbonate escarpment (Figure 3a; McIlreath & James, 1978). Parallel and continuous seismic reflections stack aggradationally representing the growth of the carbonate platform and the seismic characteristics and structural geometry of the platform remain consistent throughout deposition of this unit (Figure 3a). An exception to this seismic character is observed on the most distal *ca.* 500 m tip of the interfluve between canyons E and H, where the top Aptian surface has a chaotic, undulating, beaded response, very similar in seismic expression to structures interpreted as karst in the Tarim Field (Ruizhao & Jenkyns, 2017). Martin et al. (2010) and Clayburn et al. (2017) found similar features in the top of the carbonate platform adjacent to the study area. Seismic reflections did not indicate any reef body characteristics.

Only one major NNE-trending post-depositional normal fault is observed in the south of the study area within the carbonate platform with minor offset (*ca.* 50 ms TWT). The time-equivalent deposits in the basin are thinner than the carbonate platform (*ca.* 1,200 versus 1,800 ms TWT maximum thickness, Figure 3a), onlapping the carbonate platform interfluve. This architecture can be classified as an escarpment bypass margin considered to be a decoupled sedimentary system, where a bypass surface of non-deposition separates coeval platform margin and slope-to-basin deposits (Playton et al., 2010).

Stratal evolution can be used for further classification of escarpment margins as *inherited* or *growth* (Playton et al., 2010). Figure 3a shows the progression from an accretionary margin with coupled systems (i.e. Lower Jurassic, Morocco—Kenter & Campbell, 1991) to escarpment stratal patterns indicating a growth escarpment margin (Playton et al., 2010). The carbonate platform did not form above high-relief antecedent topography as indicated by the relatively sub-parallel seismic reflection of the acoustic basement above extended continental crust (Mourlot, Calvès, et al., 2018; Mourlot, Roddaz, et al., 2018). The subsequent post-carbonate platform margin structure and depositional

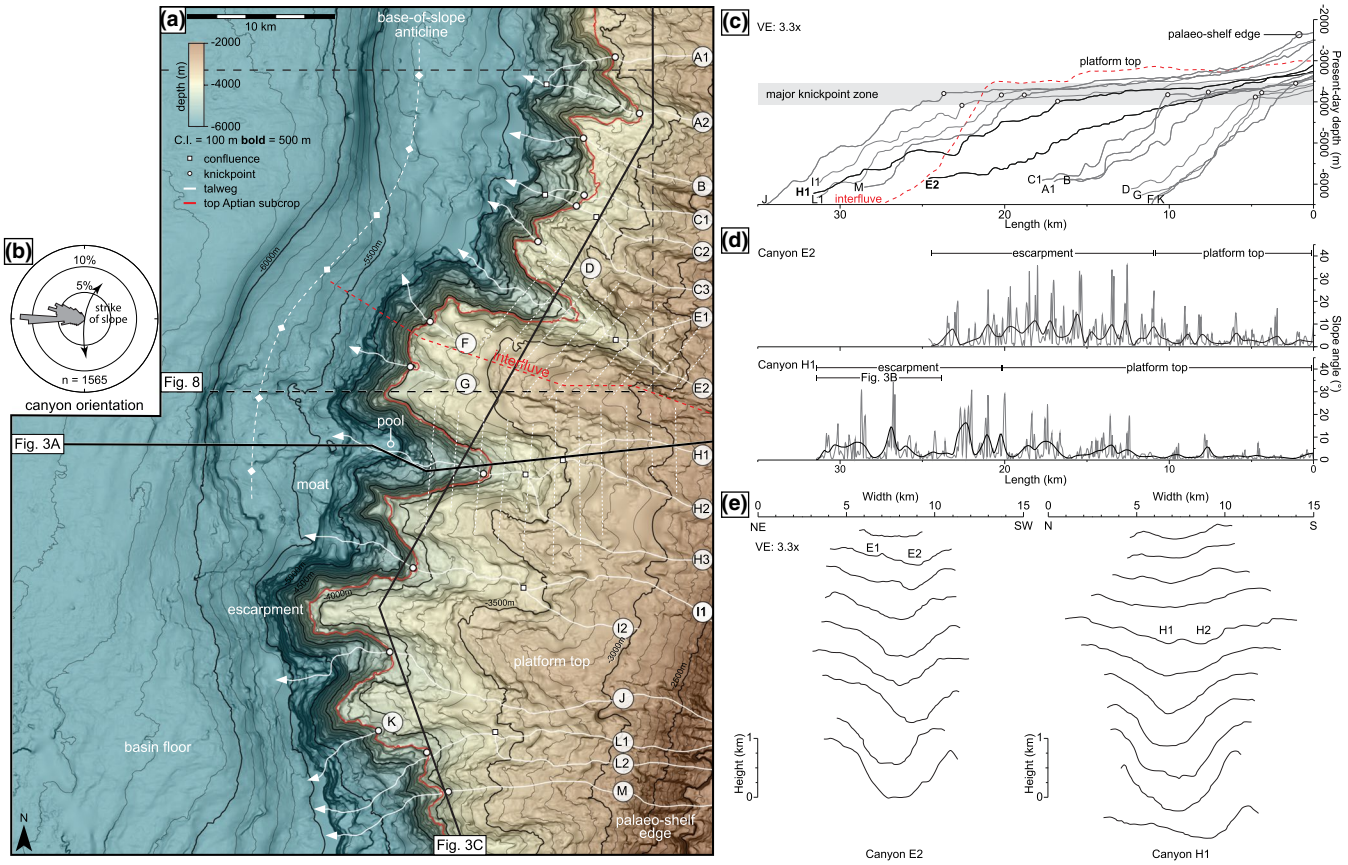

FIGURE 6 (a) Depth structure map (contours), draped over a dip magnitude map, showing the regional composite unconformity (RCU) surface and the heavily canyonised carbonate escarpment margin. Arc Hydro™ computed flow pathways are displayed (solid white lines), lettered and cross-referenced in the following figures. (b) Rose diagram showing the flow direction of each vertices from the flow pathways. (c) Talweg longitudinal slope profiles of 13 canyons and an interfluve surface shown in (a). A major knickpoint zone exists between −3,600 and −4,100 m present-day depth (shown in grey shading) corresponding to the change in lithology at the subcrop of the top carbonate, see (a). (d) Slope angle versus length along talweg longitudinal profile for two major canyons. Fine line sampled every vertices, bold averaged over 10 vertices. (e) Canyon cross-profiles sampled every 1.5 km along the talweg longitudinal profile, locations displayed on (a) (white dashed lines)

systems were heavily influenced by this early stratal architecture and the inflection point in the slope profile.

4.3 | Shelf-edge delta evolution

Overlying the carbonate platform, within the Albian interval, are a series of oblique to sigmoidal-shaped seismic reflections interpreted as prograding delta-scale clinoforms (242 ms TWT, *ca.* 330 m height; Figures 3a and 5a,b). On dip sections, mapping the clinoform rollover shows an overall 5.5 km advance that indicates progradation towards the shelf margin (west) with minor late-stage aggradation (Figure 4a). On strike sections, the delta has a broad lobate shape extending beyond the eastern edge of the survey. The erosive surface at the base of the delta is observed truncating parallel continuous seismic reflections (Figure 4a). The top of the delta is expressed as a relatively smooth, subhorizontal transgressive surface (T_1) identified by onlapping seismic reflections. The internal architecture of the delta is characterised by toplap and downlap stratal terminations that define a stratigraphic surface separating two smaller-scale delta lobes, numbered by age chronologically (Lobe 1 & Lobe 2; Figure 4). The term 'lobe' is used in this section (*shelf-edge delta evolution*) to refer to two distinct depositional units of a delta system, not lobes encountered in a deep-marine environment (see section *base-of-slope to basin floor deposits*). Mapping the bounding surfaces of the two delta lobes and construction of isochore maps are used to image the delta evolution (Figure 5).

The depocentre of delta lobe 1 is located centrally within the study area, in a more proximal position on the shelf than delta lobe 2 (Figure 5). Lobe 1 shows significant thinning towards the shelf edge (RCU truncation) with discrete areas of sediment accumulation scattered across the distal prodelta, potentially representing the infill of subaqeous channel systems (Figure 5a). Deposition appears focused at the delta front during the deposition of both lobes represented by the thickest deposits (Figure 5). Lobe 2 is volumetrically greater than Lobe 1 and progrades further into the basin. Clinoforms

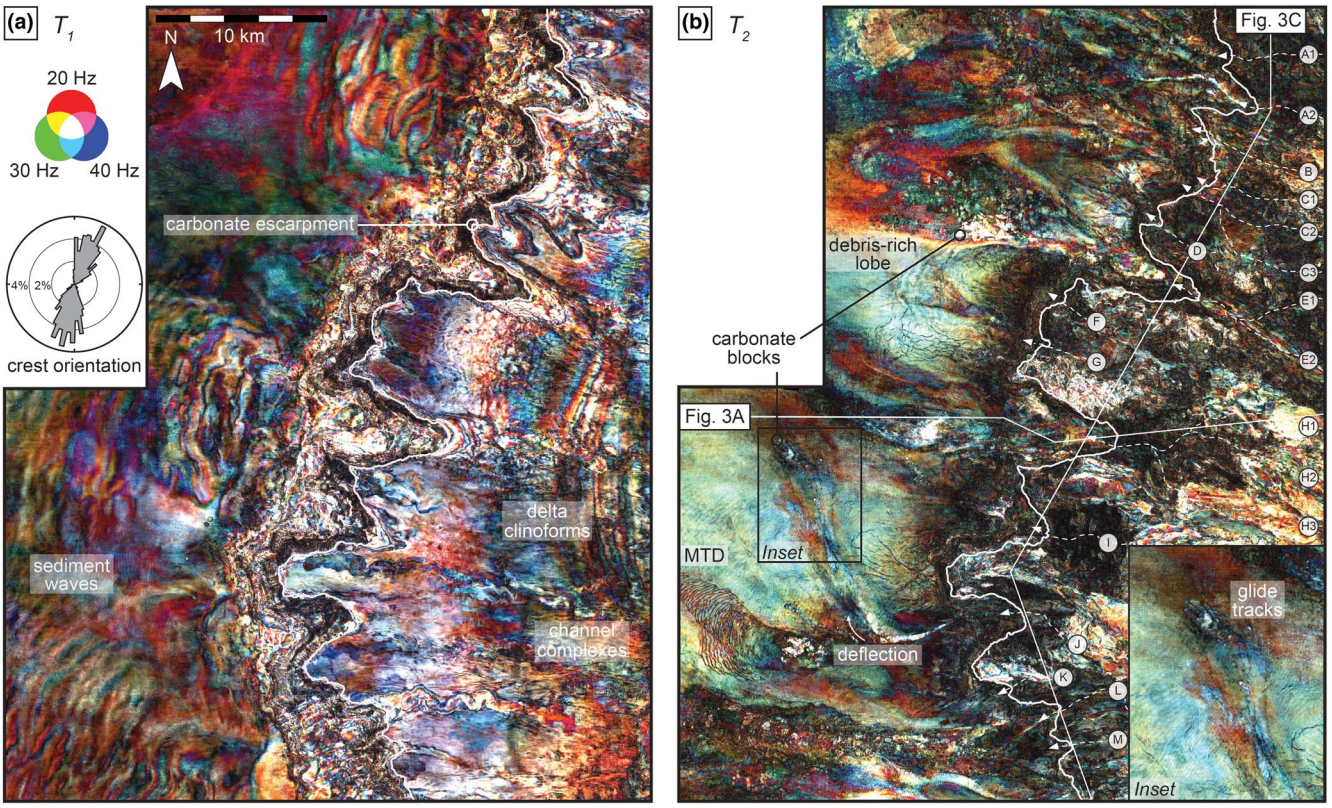

FIGURE 7 Spectral decomposition at 20, 30 and 40 Hz extracted on two surfaces, Albian-aged T_1 (a) and Late Cretaceous-aged T_2 (b), see Figure 3a for the seismic horizons mapped. These images document the two phases of margin evolution. (a) Inset rose diagram showing the orientation of each vertices from the sediment-wave crest polylines. Carbonate escarpment mapped (white line). (b) Inset zoom in on the basinal area showing glide tracks and carbonate blocks

in lobe 2 slightly downstep and show offlap geometries (Figure 4a) resulting in thinning of Lobe 2 to the east of the lobe 1 clinoform rollover as a result of compensational stacking (Figure 5b).

The presence of delta-scale clinoforms in close proximity to the shelf edge and the characteristic morphology is indicative of a shelf-edge delta, comparable to examples from the Gulf of Mexico (i.e. Sylvester et al., 2012). The delta prograded across the relict carbonate escarpment margin (e.g. Steel, Porebski, Plink-Bjorklund, Mellere, & Schellpeper, 2003). The clinoforms have a lobate-to-arcuate planform shape, identified in the tripartite classification scheme of Galloway (1975) as being a likely wave-influenced fluvial system (Figures 4 and 6a). Further characterisation following the criteria defined by Patruno, Hampson, and Jackson (2015) suggests the geometry of the clinoforms is indicative of subaqueous deposition in a stepped deltaic system. Therefore, the palaeo-water depth at the subaqueous clinoform rollover would not be more than 60 m on the shelf, increasing outboard onto the outer shelf (Patruno et al., 2015).

Beyond the delta clinoforms, multiple subaqueous channel complexes, with a maximum width of *ca*. 320 m, are observed migrating across the remainder of the shelf (Figure 7a), with their infill forming accumulations in the pro-delta apron (Figure 5). These channels form highly sinuous systems present across the entire shelf, indicating there was no significant palaeo-topography capable of diverting or capturing the channels in this interval between the delta and palaeo-shelf edge. Most channels appear linked to Lobe 2, however, earlier channels in this pro-delta area may have been cannibalised by subsequent channels associated with Lobe 2. Due to erosion by the RCU, the terminus of the channel systems cannot be observed, although approximately half are observed to be offset from the canyon axes, indicating these channels did not contribute to the initial formation of the observed later canyon systems.

4.4 | Canyon incision

Prior to major canyon incision, the upper part of the continental slope would have had two contrasting subcropping lithologies separated at the top Aptian subcrop surface (Figures 2, 3a and 6a). Carbonate sediments would outcrop on the exposed escarpment, however, to the east at the top Aptian subcrop (Figure 6a), siliciclastic sediments introduced by the shelf-edge delta system and overlying transgressive sediments would be present (Figure 3a).

Hence, later canyonisation eroded into a variable-lithology palaeo-seafloor. The palaeo-topography and margin geometry of the study area in the Aptian can be characterised as a low-relief platform top/shelf. This extends to the steep carbonate escarpment that has an average dip angle of 18.8°, with a maximum angle of 83.3° in the canyon walls and a relief from basin floor to shelf of up to *ca*. 1.5 km (Figure 6a). Slope gradient increases significantly to the west and downdip of the sub-cropping top Aptian surface before flattening out on to the basin floor.

4.5 | Quantitative seismic geomorphology

Analysing the flow pathways over the RCU surface reveals 13 submarine canyons or tributaries (A1–M) that are orientated perpendicular to the margin (Figure 6a,b). The main flow pathway trend is to the west (Figure 6b), with a minor WNW trend primarily observed in the north of the dataset. These features variably erode into the underlying stratigraphy along a *ca*. 56 km length of the slope with an average spacing of *ca*. 4 km. This average canyon spacing is significantly smaller than any modern-day canyon systems as recorded by Harris and Whiteway (2011; data resolution 1–2 km), with the average value for modern canyon spacing on continental margins worldwide being 39 km.

Canyons and associated erosion at this stratigraphic level extend beyond the limit of the study area (Figure 1), as indicated to the north (Martin et al., 2010) and south (Mourlot, Calvès, et al., 2018; Mourlot, Roddaz, et al., 2018). Mounded interfluves are preserved, with the largest having a maximum area of *ca*. 75 km^2 between canyons E2 and H1 (Figure 6a). The canyons have relatively straight profiles (average sinuosity—1.09; Table 1) with an average canyon length of 18.3 km (Figure 6c and Table 1). Canyon width was measured every 1 km along the talweg profiles revealing an average width of 3.1 km and maximum value in canyon H2 of 8.3 km (Table 1). Two canyon profiles are displayed in Figure 6e to illustrate the change from proximal broad low-relief U-shaped profiles to narrow V- and U-shaped profiles further downslope, as slope angle increases from the low-gradient platform top to the steeper escarpment (Figure 6d,e). Confluences in the canyon tributaries generally occur on the shelf, where branching tributaries join to form larger conduits (Figure 6a). A zone of major knickpoints occurs between 3,600 and 4,100 m present-day depth where the talweg slope profile rapidly steepens (Figure 6c); overall, these profiles are convex in shape. This knickpoint zone is at the maximum limit of progradation reached by the underlying shelf-edge delta. The spatial relationship between the knickpoints and the top Aptian subcrop illustrates that substrate lithology is one of the primary controls on slope angle within canyons and their interfluves.

4.6 | Canyon classification

Canyon classifications have been developed following the early identification of submarine canyons by Shepard (1934). Submarine canyons are typically classified based on the degree of incision into the shelf and slope (Twichell & Roberts, 1982; Farre, McGregor, Ryan, & Robb, 1983; Brothers, Uri, Andrews, & Chaytor, 2013; e.g. siliciclastic system—Jobe, Lowe, & Uchytil, 2011; mixed system—Puga-Bernabéu, Webster, Beaman, & Guilbaud, 2011; global review—Harris & Whiteway, 2011) and/or morphological criteria (Tournadour et al., 2017). A geomorphological approach was proposed by Puga-Bernabéu et al. (2011). Jobe et al., (2011) proposed a more holistic classification incorporating depositional processes and canyon fill. In this study these methodologies have been combined to provide a template for the classification of the canyons offshore The Gambia, the key discriminator being whether the canyons incise the shelf or not. This allows definition of two primary types; (a) shelf-incised and (b) slope-confined systems (otherwise known as blind or headless canyons, Amblas et al., 2006). We further subdivide shelf-incised canyons dependent on the degree of erosion within the canyon long profile, as: 1A. graded versus 1B. ungraded (Mitchell, 2005). Previous workers have suggested that slope-confined and shelf-incised canyons represent the primary and secondary stages, respectively, of canyon evolution, potentially indicating the relative ages of canyons along the margin (Dingle & Robson, 1985; Klaus & Taylor, 1991; McGregor, 1985; Nelson & Maldonado, 1988).

Based on our classification, Table 1 summarises the main geomorphological parameters extracted from the canyonised RCU surface (Table 1; Figure 6a). Shelf-incised canyons erode into the shelf and extend a greater distance from the escarpment margin (average distance eroded from palaeo-shelf edge 15.7 km), whereas slope-confined canyons are confined to the escarpment. Only two canyons display the characteristics of graded shelf-incised canyons based on their relatively smooth long profiles in Figure 6c, canyons E2 and H1; the remainder have irregular concave upwards profiles. Canyon heads vary from pointed (slope-confined canyons) to amphitheatre-shaped at the palaeo-shelf edge (Figure 6a), however, the dataset does not cover the upper reaches (origin) of these canyons in the north. Canyon width, length and incision depth commonly decreases from graded to ungraded shelf-incised canyons to slope-confined canyons (Table 1).

4.7 | Formation processes

Two models are proposed and well supported by modern day examples for the formation of canyons on continental margins (summarised in Pratson et al., 2007): downslope erosion (Daly, 1936) and retrogressive failure (Farre et al., 1983;

Twichell & Roberts, 1982). Downslope erosion by sediment gravity flows with a variety of trigger mechanisms create incisions in the slope, subsequently enlarged by later flows to establish a canyon; and retrogressive failure, a result of mass movement due to slope failure that migrates erosion upslope. These processes propagate in opposite directions, can occur coevally (Pratson & Coakley, 1996) and vary through time. The type of canyon also controls the amount of potential sediment catchment at the canyon head and hence the degree of erosion by downslope processes. Shelf-incising canyons are able to capture sediment from a larger 'catchment area` compared to slope-confined systems (Jobe et al., 2011). The architecture of the canyons in this dataset is the final result of these cumulative processes and as such, each canyon represents various stages of canyon development. To investigate the morphological evolution and formational processes of each canyon, deposits at the terminus of the canyons have been studied, and are described in the following section.

4.8 | Base-of-slope to basin floor deposits

4.8.1 | T_1—Sediment waves

Surface T_1, of Albian age, is the maximum flooding surface overlying the Albian delta (Figures 4 and 7a). Sediment waves (sensu Wynn & Stow, 2002) characterise these deposits in the base-of-slope to basin floor (Figure 3b and 7a). Three areas of sediment waves are observed; in the north of the dataset (between canyons A to C; minimum spatial extent—326 km^2); centre (H to I; 255 km^2) and to the south (K to M; 365 km^2; Figure 7a). This depositional system is imaged in Figure 3b showing the characteristic asymmetrical, undulating bedforms and decreasing in wave dimensions basinward. Average wavelength is *ca*. 325 m and average trough-to-crest height is *ca*. 15 m. Orientation data extracted from digitised wave crests show a dominant NNE-SSW trend, aligned parallel to the strike of the regional slope (Figure 7a). A 10-km-long moat is present at the base of the escarpment margin (Figure 3b), separating the sediment wave field from the escarpment. Crest curvature has an upslope convexity, possibly indicating up-current migration (i.e. antidunes; Fildani et al., 2013; Fildani, Normark, Kostic, & Parker, 2006; Wynn, Masson, Stow, & Weaver, 2000b). Following the classification of Wynn and Stow (2002), we propose that these sediment waves likely formed by downslope-flowing turbidity currents originating from subaqueous channel complexes imaged in Figure 7a (Fildani et al., 2013). However, this classification is based on geomorphological parameters of sediment waves and deducing their formative processes remains unclear (McCave, 2017). Cretaceous contour-parallel currents have been postulated along this margin (Mourlot, Calvès, et al., 2018; Mourlot, Roddaz, et al., 2018). Without lithological calibration, we can only postulate based on the morphology described that the systems are fine grained (sensu Wynn & Stow, 2002).

4.8.2 | T_2—Margin collapse

The T_2 surface is Late Cretaceous in age, and illustrates a variety of deposits in the basin associated with the margin collapse (Figure 7b). A total of 58 geobodies at the base-of-slope to basin floor are interpreted through 200 horizon slices from the top Aptian to the base Tertiary unconformity surface, and geomorphological data extracted (Table 2). The spectral decomposition of surface T_2 allows the visualisation of some of these depositional systems and facies (Figure 7b). Two end-member styles of lobate deposits are observed originating from canyons (Figure 8). Earlier lobes are predominately debris-poor, lacking seismically resolvable blocks and have an elongate lobate shape (Figure 8a). Whereas later lobes are debris-rich containing blocks of the eroded carbonate platform up to 0.92 km^2, with some blocks observed beyond the lobate bodies termed 'outrunner blocks' (Figure 8b). In total, three seismic facies dominate in this region, lobes (debris-poor versus debris-rich; Figure 8) and MTDs.

Based on these observations, we interpret that the debris-poor lobes were likely deposited predominantly by turbidity current processes and the debris-rich lobes by debris flows (McHargue, Hodgson, & Shelef, 2019). The degree of mixing will be difficult to distinguish without lithological data (Talling, 2013). There is an apparent lack of any base-of-slope or basin floor channel-levee systems that usually characterise the lower courses of canyons in submarine fan systems in the study area (e.g. Covault, 2011; Galloway, 1998). However, these are present further north and south of the study area where there is higher siliciclastic sediment supply (Mourlot, Calvès, et al., 2018; Mourlot, Roddaz, et al., 2018). The basinal deposits form a strike-discontinuous apron that are interpreted to nearly all originate from point sourced canyon systems interpreted upslope (Playton et al., 2010). Off-canyon axes, there are abundant polygonal faults in the base-of-slope signifying background apron mud-rich deposits (Figure 8b; Cartwright & Lonergan, 1996).

The number and volume of debris-poor lobes and run-out distances are minor in comparison to the contribution to the slope apron by the two other facies (Table 2). The average debris-poor lobe run-out distance is *ca.* 9.9 km and limited to the most proximal position in the base-of-slope, forming narrow elongate lobes characterised by high-amplitude seismic reflectors (Figure 3b). In Figure 3b, there are multiple horizons with similar acoustic properties and geometries suggesting vertical lobe stacking over numerous depositional events.

TABLE 2 Geomorphological data extracted from the PaleoScan™ horizon stack and interpreted geobodies. Bold values signify the deposit extended beyond the study area. DP, debris-poor lobes; DR, debris-rich lobes; MTD, mass transport deposit

ID	Horizon		X (m)	Y (m)	Depth (msTWT)	Facies	Run-out length (km)	Max. width (km)	Length:Width ratio	Surface area (km^2)	Mean thickness (m)	Volume (km^3)
	Start	End										
A1	108	113	200,763	1,502,457	4,723	DP	5.5	1.5	3.6	16.5	79.6	0.5
A											Cumulative	0.5
B1	107	111	199,452	1,500,218	4,759	DP	9.8	2.6	3.8	53.9	45.7	0.9
B2	116	121	199,029	1,501,318	4,734	DP	9.7	3.9	2.5	65.2	82.7	2.1
B3	122	131	188,413	1,502,100	5,478	DR	16.6	5.7	2.9	204.5	109.8	7.0
B4	132	141	196,302	1,501,863	4,665	DR	17.8	6.6	2.7	222.8	173.1	14.8
B5	142	152	195,398	1,503,254	4,663	DP	15.6	1.7	9.4	65.4	56.1	1.5
B6	164	171	199,694	1,500,772	4,277	DR	8.6	4.0	2.1	73.2	120.0	2.2
B											Cumulative	28.4
C1	108	114	197,035	1,492,787	4,925	DP	7.2	1.8	4.0	36.5	110.4	1.4
C2	119	126	196,020	1,493,767	4,888	DR	8.8	2.9	3.1	168.3	101.9	3.9
C3	127	129	197,031	1,492,349	4,709	DR	20.7	8.5	2.4	237.6	55.0	6.6
C4	130	140	189,403	1,496,527	5,242	DR	24.8	9.4	2.6	444.1	137.2	21.4
C5	149	162	192,498	1,497,264	4,771	DR	21.5	10.4	2.1	651.9	154.3	24.3
C6	163	172	185,669	1,496,969	5,228	MTD	**28.2**	7.2	3.9	680.7	180.9	42.2
C7	183	195	185,450	1,498,035	4,937	DR	**33.6**	8.7	3.8	744.8	181.2	34.8
C											Cumulative	134.6
D1	96	101	199,173	1,490,987	4,761	DP	2.7	1.2	2.3	8.2	59.4	0.2
D2	130	136	197,446	1,491,373	4,656	DR	5.1	1.5	3.4	26.9	68.2	0.7
D											Cumulative	0.9
E1	107	119	188,178	1,492,209	5,586	DP	15.4	4.9	3.2	154.3	98.6	5.6
E2	120	122	184,646	1,492,399	5,636	DR	19.5	5.6	3.5	129.7	56.2	3.4
E3	123	129	189,299	1,489,058	5,264	DP	13.1	2.5	5.3	60.7	57.1	1.5
E4	130	139	181,938	1,490,594	5,523	DR	**24.3**	8.2	3.0	393.3	151.1	22.1
E5	141	166	181,245	1,498,573	5,106	DR	**26.8**	11.9	2.2	504.3	170.2	29.0
E6	171	176	190,026	1,488,398	4,762	DR	25.0	6.4	3.9	270.1	91.5	8.7
E7	188	196	188,505	1,488,920	4,691	DR	23.3	12.2	1.9	520.4	126.0	16.0
E											Cumulative	86.3
F1	113	114	191,154	1,485,262	4,968	DP	5.0	2.8	1.8	22.0	27.2	0.2

(Continues)

TABLE 2 (Continued)

ID	Horizon		X (m)	Y (m)	Depth (msTWT)	Facies	Run-out length (km)	Max. width (km)	Length:Width ratio	Surface area (km^2)	Mean thickness (m)	Volume (km^3)
	Start	End										
F											Cumulative	0.2
G1	100	101	183,938	1,485,561	5,665	MTD	11.7	6.7	1.8	141.1	22.0	1.7
G2	104	104	187,064	1,482,395	5,348	MTD	5.5	2.3	2.4	17.2	34.4	0.4
G3	105	106	187,254	1,482,224	5,280	DP	6.3	2.6	2.4	32.7	50.8	1.0
G4	112	116	184,643	1,484,928	5,440	DR	12.3	6.4	1.9	106.9	60.4	2.7
G5	121	124	182,537	1,484,961	5,510	MTD	10.1	4.4	2.3	74.8	51.9	2.2
G6	134	148	182,801	1,483,137	5,233	DR	14.3	5.7	2.5	157.6	113.3	5.9
G7	160	168	182,748	1,483,411	5,132	DR	**15.3**	3.6	4.2	170.2	140.0	8.0
G8	182	186	186,578	1,481,605	4,685	DR	11.4	3.7	3.1	64.9	77.3	2.3
G											Cumulative	24.2
H1	110	119	184,875	1,474,506	5,368	DP	13.8	4.8	2.9	135.0	116.2	4.0
H2	121	129	180,111	1,473,824	5,518	DR	19.0	6.9	2.7	193.7	83.0	6.4
H3	130	133	183,366	1,472,873	5,325	DP	12.6	3.3	3.8	85.9	50.9	1.7
H4	134	146	180,575	1,475,729	5,286	DR	**25.6**	12.9	2.0	702.6	202.3	40.5
H5	154	165	178,233	1,477,520	5,354	DR	**30.6**	16.3	1.9	924.7	149.7	41.7
H6	175	182	182,311	1,475,898	4,863	DR	**28.0**	11.0	2.5	603.1	142.8	38.5
H7	184	186	183,588	1,475,923	4,737	DR	**19.6**	7.0	2.8	210.1	57.5	4.7
H8	189	199	183,726	1,477,954	4,452	DR	**26.7**	14.7	1.8	644.8	142.7	21.2
H											Cumulative	158.7
I1	101	102	182,641	1,468,193	5,584	DP	8.0	3.6	2.3	34.6	30.2	0.6
I2	103	108	178,829	1,470,804	5,740	MTD	6.2	3.4	1.8	52.5	84.3	1.6
I3	113	115	176,741	1,470,895	5,827	DR	**20.0**	6.5	3.1	193.8	68.6	4.9
I4	116	121	182,771	1,468,794	5,502	DP	11.6	2.5	4.6	71.9	63.0	1.4
I5	153	159	179,142	1,468,807	5,338	MTD	10.8	4.9	2.2	136.1	176.7	4.4
I											Cumulative	12.8
J1	106	112	174,733	1,464,514	5,811	MTD	**24.6**	5.9	4.2	368.4	98.1	18.0
J2	113	118	177,207	1,458,130	5,581	DR	16.9	3.5	4.8	158.9	116.3	6.6
J3	121	132	178,707	1,458,249	5,342	DR	18.5	5.8	3.2	431.7	143.2	19.9
J4	133	136	170,788	1,457,035	5,529	MTD	17.2	4.3	4.0	173.6	52.0	3.7
J5	137	148	172,181	1,463,303	5,531	DR	**22.5**	9.7	2.3	580.2	91.6	12.8
J6	149	154	176,916	1,463,641	5,320	DR	20.5	5.9	3.5	340.7	92.4	8.3

(Continues)

TABLE 2 (Continued)

ID	Horizon		X (m)	Y (m)	Depth (msTWT)	Facies	Run-out length (km)	Max. width (km)	Length:Width ratio	Surface area (km^2)	Mean thickness (m)	Volume (km^3)
	Start	End										
J7	159	161	172,698	1,462,945	5,385	DR	20.5	9.6	2.1	376.2	63.2	10.6
J											Cumulative	79.9
L1	113	122	174,606	1,450,949	5,575	DR	**24.9**	8.1	3.1	698.4	150.7	26.6
L2	126	139	173,361	1,449,075	5,479	DR	**27.8**	10.4	2.7	758.2	159.7	34.1
L3	142	147	173,626	1,455,419	5,368	DR	**25.4**	11.9	2.1	521.3	71.5	11.7
L4	164	172	175,838	1,454,565	5,170	DR	**27.0**	11.6	2.3	941.4	114.8	27.5
L5	172	179	171,144	1,451,153	5,226	DR	**26.9**	13.1	2.1	638.3	178.5	18.9
L6	182	196	171,233	1,453,421	5,034	DR	**28.0**	13.0	2.2	632.3	131.0	24.7
L											Cumulative	143.5
					Mean	DP	9.9	2.8	3.8	62.2	69.0	1.6
						DR	21.0	5.5	2.7	184.3	98.5	7.5
						MTD	14.3	6.0	3.1	227.4	95.5	10.1
						Total	17.4	7.5	3.2	321.5	112.5	13.3

Throughout the stratigraphy, eight discrete geobodies are identified with a complex and chaotic internal character, compressional ridges and imbricate thrusts at their toe, basal scoured shear surfaces that distinguish them from the debris-rich lobes as MTDs (sensu Moscardelli & Wood, 2016; i.e. Figure 7b). These are mostly detached from the escarpment margin and occur dispersed throughout the interval. Two types exist: point-sourced MTDs associated with a local canyon system, and MTDs developed on the basin floor, both having similar geomorphological features, but different origins. A confined MTD point sourced from canyon J is identified with a run-out distance of 23.6 km (Figure 7b), compressional ridges are present in the distal toe region of the MTD and large blocks are observed proximally. This feature formed basin floor topography that was capable of deflecting the overlying debris-rich lobe to the north (Figure 7b). Run-out distances of all MTDs average *ca.* 14.3 km, with average volumes of 10.1 km^3 (Clare et al., 2019; Table 2). These values are comparable to the values reported from a global compilation of MTDs by Moscardelli and Wood (2016). Clear basal shear surfaces and imbricate thrusts are imaged in Figure 3b. In this example the MTD appears to be related to the compressional deformation at the base of the escarpment margin increasing the gradient of the sea-floor topography.

Volumetrically the most significant facies contribution to deposition in the base-of-slope to basin floor are debris-rich lobes (volume of debris-rich lobes is 573.3 km^3 from a total of 669.8 km^3, 86%), with run-out distances commonly beyond the extent of the dataset (Figures 7b and 8b). The lobate planform morphology is similar in appearance to unconfined submarine fans (Prélat, Covault, Hodgson, Fildani, & Flint, 2010), but the abundance of 100-m-scale high-amplitude blocks suggests these flows are debris-rich (isolated basinal megabreccia sensu Playton et al., 2010). The blocks are interpreted as eroded blocks of the lithified carbonate platform based on their observed glide tracks in the underlying stratigraphy (Figure 7b; Bull, Cartwright, & Huuse, 2009; Hurd, Kerans, Fullmer, & Janson, 2016). These denser flows, where there is suspension of particles in a viscous matrix, are likely to contribute to more erosion (Mitchell, 2006). Mapping 36 debris-rich lobes indicates they are exclusively point sourced from canyon mouths.

4.8.3 | Spatiotemporal evolution

The earliest deposits associated with the initiation of the canyon systems are spatially distinct. In the north and central areas deposits are dominated by debris-poor lobes for a significant period of time (av. 10 horizon slices, *ca.* 1 myr, Figure 9). The southern sector is

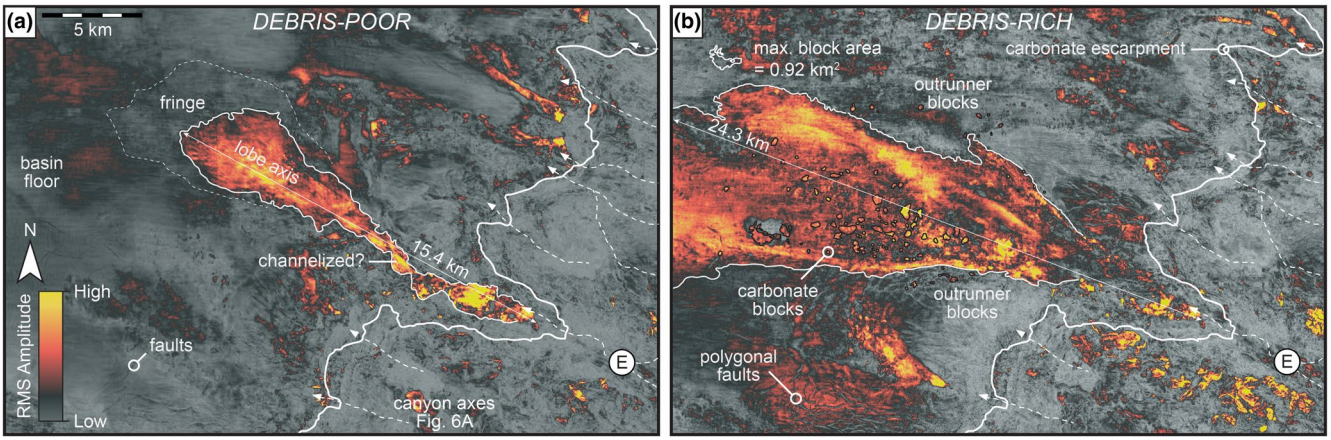

FIGURE 8 RMS amplitude maps extracted from a ± 12 ms window around an intra-Albian horizon (A) and T_1 (B), displaying the two end-member types of lobes (debris-poor versus debris-rich). Location of the maps is shown in Figure 6a

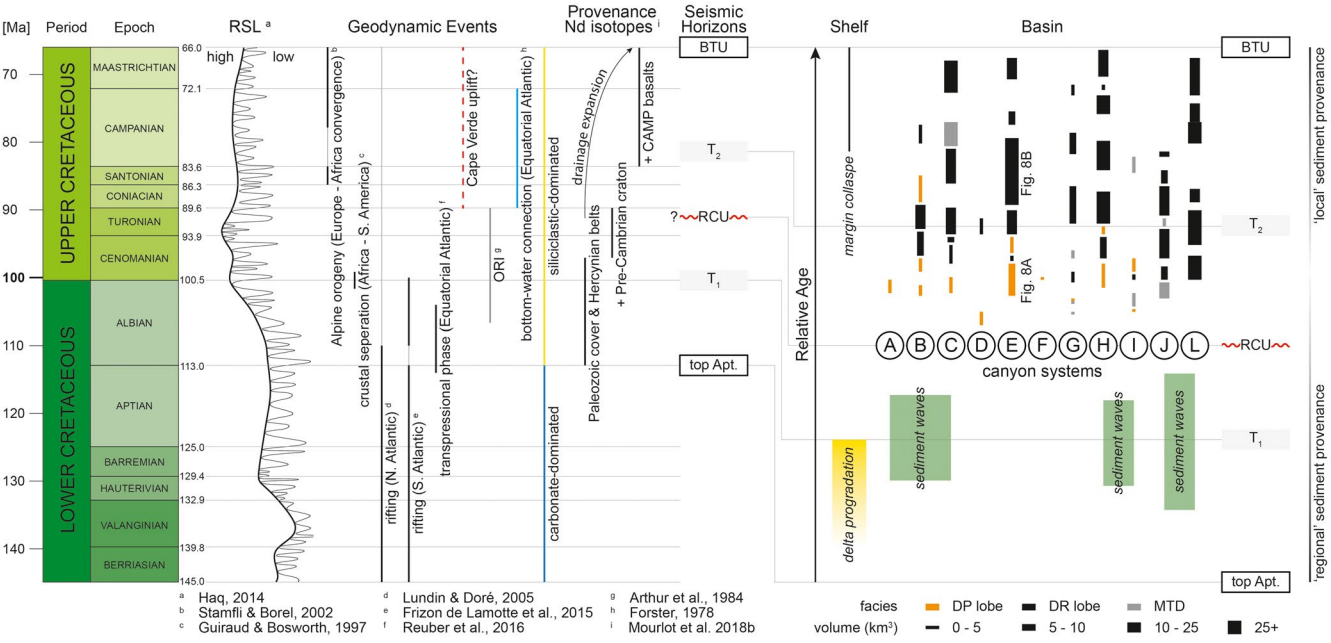

FIGURE 9 Summary of depositional systems active on the platform and in the basin through time, linked to each canyon system displayed in Figure 6a. The line thickness indicates the volume of each geobody/deposit. Canyon K is omitted as this directly feeds the amalgamated basin system of canyon L and M. Canyon M is also omitted as the majority of the associated deposits are beyond the dataset. This was created through the interpretation of a 200-surface horizon stack generated in PaleoScan™ between the top Aptian and base Tertiary unconformity. The stratigraphic surfaces T_1 and T_2 are indicated. This is correlated with the geodynamical events effecting the Central Atlantic, with references shown. BTU, Base Tertiary Unconformity; DP, debris-poor lobes; DR, debris-rich lobes; MTD, mass transport deposit; ORI, organic-rich interval; RCU, regional composite unconformity; RSL, relative sea level

dominated by MTDs (Figure 9). This indicates that the erosional processes responsible for generating canyons varies along strike of the margin. This also suggests that at this time, the main sediment source input from the shelf was captured by canyons in the north and central areas. Heterogeneous basinal deposition is strike discontinuous, with canyons recording simultaneous deposition of different seismic facies (i.e. debris-rich lobe—canyon E, and MTD—canyon J; Figure 7b). The discontinuous nature of the sedimentation signifies strike-limited points of instability and subsequent collapse of the margin (Playton et al., 2010). A comparison can be made to the collapse of the Famennian-aged escarpment margin in the Canning Basin, Australia (George, Playford, & Powell, 1995), where a similar 1–10 s km spacing between collapse deposits is recorded. Offshore The Gambia, canyon deposits evolve from debris-poor to debris-rich lobes and MTD deposits, as recorded in the evolution of the basin floor stratigraphy downslope of canyons offshore New Jersey (Pratson & Coakley, 1996).

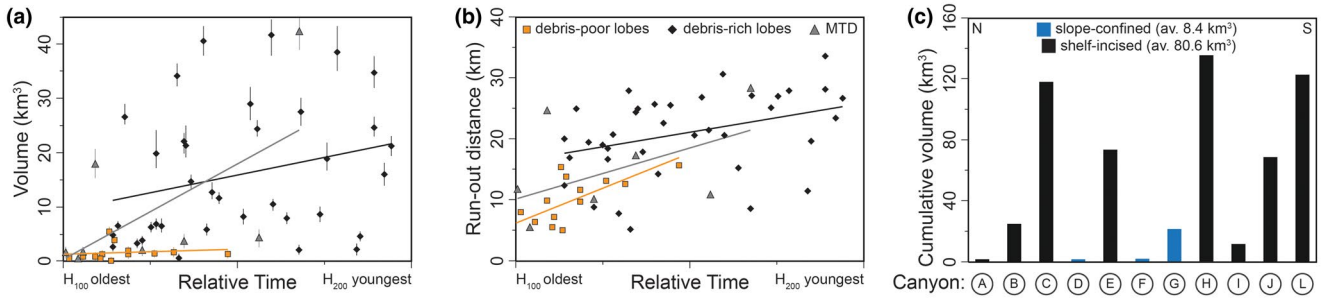

FIGURE 10 (a) Volume of deposit (derived from geobody interpretation) plotted with uncertainty against relative time (estimated from the PaleoScan™ horizon stack, i.e. horizon 100–200 from oldest to youngest), coloured by facies. (b) Run-out distance plotted against relative time. Trend lines coloured by facies. (c) Cumulative volumes of sediment transported through each canyon system

Plotting the volume of each geobody/deposit against relative time shows a weak positive relationship, suggesting the intensity and scale of margin collapse increased towards the end Cretaceous, supported by the general increase in run-out length through time (Figure 10a,b & Table 2). This may also reflect an increase in sediment supply to the margin. These are large volumes that are significant contributors to base-of-slope sedimentation (Moscardelli & Wood, 2016). However, the overall frequency of events decreases through this period. Collapse frequency is higher in the shelf-incised than slope-confined canyon systems (Figure 9); conceivably due to the capture of more shelfal sediment causing further slope erosion and instability.

The run-out distance increases through time for all facies (Figure 10b), mass wasted deposits (MTDs and debris-rich lobes) increase to a maximum run-out for a debris-rich lobe of 33.6 km from canyon C, extending beyond the study area. Slope-confined canyons transport significantly less volume of sediment to the basin in comparison to shelf-incised canyons; the estimated average volume of sediment transported through slope-confined canyons is an order of magnitude lower than shelf-incised systems (average volume per canyon 8.4–80.6 km^3, respectively; Figure 10c; Table 2). If we assume all sediment deposited in debris-poor lobes is bypassed to the base-of-slope from regional sources, i.e. shelf-edge deltas, and sediment deposited in debris-rich lobes to be derived solely from the escarpment margin, a comparison of the total volume of sediment delivered from regional/extra- and local/intra-basinal sources is 21.8 and 648.0 km^3, respectively, during the Late Cretaceous.

5 | DISCUSSION

5.1 | Mixed system margin morphology

The inherited Late Cretaceous slope morphology of The Gambian continental margin is a complex product of mixed depositional systems that have evolved through the Mesozoic. From carbonate margin growth (top Aptian), subsequent demise associated with siliciclastic influx from a shelf-edge delta system (Albian), transgression during the Cenomanian and ultimately Late Cretaceous margin collapse (summarised in Figure 9).

Spatial variability in siliciclastic input is a major control on the location and health of carbonate factories, which strongly influences continental margin morphology (Moscardelli et al., 2019). The study area is located in a region that received siliciclastic-dominated sedimentation post-Aptian times delivered by a shelf-edge delta, whereas beyond this area we predict margin morphology may have continued to be controlled by carbonate deposition where siliciclastic sediment input was low. In those areas, there may be other allogenic controls on the regional demise of the carbonate platform, i.e. climate, nutrient availability and rapid sea-level rise. Similar spatial heterogeneity of a mixed system recorded on the shelf is documented on the conjugate US–Canadian margin in the Baltimore Canyon trough (Meyer, 1989) and Shelburne sub-basin, Nova Scotia (Moscardelli et al., 2019).

The depositional evolution established a significant lithological contrast in the subcrop on the slope prior to later canyonisation, which had an important regional control on the subsequent inflection in the slope (Hurd et al., 2016), location of knickpoints within canyons and the nature of the seafloor substrate eroded. This is comparable to slope morphology observed on the present-day conjugate U.S. Atlantic continental margin, where steep subcropping Mesozoic limestone escarpments have up to 2 km of relief, and shape the Blake Escarpment seascape (Jansa, 1981; Land, Paull, & Spiess, 1999). The lithological properties and seismic character of the carbonate margin imply heterogeneous carbonate lithologies cropped out on the seabed of the escarpment during canyon incision, generating rugose seafloor topography. Horizontal limestone benches form angular ledges in the face of the Blake Escarpment, produced by lateral scarp retreat (Land et al., 1999). A comparable seafloor is envisaged during the Late Cretaceous in the study

area. Knickpoints and the slope inflection form at the siliciclastic-carbonate contact (top Aptian subcrop—Figure 6a) by simple entrenchment due to varied competence of the substrate, with similarities to knickpoints in fluvial systems (i.e. Miller, 1991). Substrate lithology is therefore one of the key controls on the slope morphology.

5.2 | Canyon incision evolution

Combining techniques adapted from hydrology with seismic facies analysis and interpretation of the basin deposits allows interpretation of the possible mechanisms of slope-confined and shelf-incised canyons initiation during the Late Cretaceous. The spatial variation in the earliest canyon-related deposits recorded in the basin stratigraphy can be used to interpret the characteristics of the early stages of canyon formation, i.e. canyons linked with debris-poor lobes are interpreted to be related to downslope eroding sediment gravity flows (northern canyons), whereas debris-rich lobe- and MTD-related canyons formed due to mass wasting processes (southern canyons; Figure 9). The relative increase in volume and frequency of gravity flow and mass wasting events is interpreted to be due to an evolution from ungraded to graded canyons (Figures 6c and 9). Pratson and Coakley (1996) show how repeated sediment flows trigger retrogressive failure, and hence headward migration of canyon erosion by downslope-eroding sediment gravity flows and grading of the submarine canyon long profile.

The subaqueous channel complexes observed associated with the shelf-edge delta are indicative of sediment transported to the escarpment margin and may have contributed to the early inception of canyons (Figure 7a). This could be another mechanism to initiate canyons that can be tied spatially to channels (Canyons L and M), however, many channels are observed to be spatially distinct from the overlying younger canyons (i.e. interfluve between Canyons H and I).

The broad lobate geometry and orientation of the sediment wave deposits in the basin downdip of the canyons (Figure 7a) suggest sediment gravity flows bypassed and eroded the early escarpment margin, forming base-of-slope aprons. Nelson, Maldonado, Barber, and Alonso (1991) recognise these apron facies on line-sourced mature continental margins, where deltas feed sediment through a gullied slope. Hence, we postulate some canyons are likely to have formed from an initial gullied slope during the progradation of the shelf-edge delta (in the Albian), in a similar maturation process documented by Farre et al., (1983) on the U.S. Atlantic continental margin. This is recorded in many siliciclastic settings (e.g. Jobe et al., 2011; Lonergan, Jamin, Jackson, & Johnson, 2013; Shumaker, Jobe, & Graham, 2017), where the seabed substrate is composed of uncompacted fine-grained sediment. However, in this study, no gullies have been observed on the RCU surface. To the west of the top Aptian subcrop, i.e. beyond the shelf-edge delta deposits, the Late Cretaceous seabed offshore The Gambia would have been relatively compact and hard, composed of lithified carbonate lithologies (Figure 6a), potentially preventing the formation of gullies (e.g. Prélat, Pankhania, Jackson, & Hodgson, 2015).

Several canyon evolution models have evolved from the preliminary findings of canyon origins by Daly (1936), and Twichell and Roberts, 1982. This has been supported by reduced-scale experimental approaches, such as that of Lai, Gerber, and Amblas (2016), that develop understanding of how unconfined sediment gravity flows form and shape submarine canyons, with progressive growth of slope relief. Findings from this model agree with the results from our analysis for canyons interpreted to have formed by downslope erosion. It would be of interest to repeat this experiment on a semi-consolidated or consolidated slope to imitate the carbonate escarpment and understand changes in canyon architecture and long profile grading, and model how basin deposits temporally evolve. In the study area, there is geomorphological and stratigraphic evidence for canyons having formed by both processes of downslope erosion and retrogressive failure.

5.3 | Sediment transfer from shelf to basin

Sediment transfer from the shelf to basin across the carbonate escarpment, and latterly through the canyonised surface of the RCU, is governed by three principal physical erosional processes: gravity flows, mass wasting and oceanographic bottom currents, in addition to chemical dissolution of carbonates. Ultimately these processes shape the architecture of the continental margin and control sediment distribution. During the Albian, the location of the main depocentre is linked to the location of the shelf-edge delta. Coarse-grained sediment is mainly trapped on the shelf, although some bypass does occur to base-of-slope aprons down canyons. This regional, extra-basinal, siliciclastic-prone source of sediment and drainage is postulated to vary laterally and may have also exerted a control over the location and health of the carbonate factories and accumulation of the platform along this mixed-system margin. Mourlot, Calvès, et al. (2018), Mourlot, Roddaz, et al. (2018) show multiple entry points for similar-aged deltaic systems (see their Figure 9b), introducing a regional source of sediment from rivers draining the onshore Senegal Basin and hinterland of northwest Africa. This sediment is likely to be very different in composition to locally derived material associated with the erosion and collapse of the margin. We postulate the local, intra-basinal sediment to be much more heterogeneous, composed of mixed re-sedimented lithified carbonate facies and siliciclastic material, in comparison to

the very fine-grained, clean sandstones and mudstones derived from the regional fluvio-deltaic input (encountered in wells Jammah-1 and Wolof-1, Figure 2). As the margin begins to collapse following establishment of the RCU in the early Late Cretaceous, locally derived sediment, developing debris-rich lobes and MTDs, dominates over sediments input from extra-basinal drainage. Much of the extra-basinal drainage sediment may have been trapped further inboard as the onshore Senegal Basin was transgressed.

A quantitative analysis of the different facies distinguishes regional (3% of total sediment transported to the basin) versus local (97%) provenance signals from the seismic geomorphology. Long-lived (*ca*. 28 Myr) sediment bypass is documented by the canyon systems interpreted in this paper (Figure 6a), facilitating sediment transfer from the shelf to basin floor. The seismic expression of the composite RCU shows entrenchment of the canyon systems rather than lateral migration, and there is a lack of evidence for multiple incisions (i.e. slope channel–levee systems – Deptuck, Steffens, Barton, & Pirmez, 2003). This forms a deeply incised surface where we assume the basal surface of the canyons (RCU) records a considerable amount of time when either complete sediment bypass occurred and/or the canyon was bypass dominated through time (sensu Stevenson, Jackson, Hodgson, Hubbard, & Eggenhuisen, 2015). The limited vertical resolution (*ca*. 20 m) of the seismic reflection data and lack of borehole data within any of the canyons documented in this study inhibits our sedimentological and stratigraphic interpretation of the deposits associated with these zones. Generally, the stratigraphic architecture of the canyon-fill has a back-stepping onlapping signature, with a low-amplitude acoustic response throughout the Late Cretaceous sequence (Figure 3). In all the wells where the RCU has been drilled, the overlying stratigraphy is mudstone dominated (Figure 2). However, it is conceivable that the canyon fill directly above the bypass surface may be thin bedded and sand prone (i.e. Stevenson et al., 2015 and references therein) below the resolution of the seismic data. From an applied perspective, the RCU surface and deposits associated with it may act as conduits for migrating hydrocarbons from the basin to the shelf, potential stratigraphic traps and/or act as thief zones in stratigraphic traps of hydrocarbons in the potential base-of-slope reservoirs (e.g. Ghana—Kelly & Doust, 2016).

5.4 | Regional controls on stratigraphic evolution

High-resolution documentation of the seismic geomorphology related to the collapse and submarine canyonisation of The Gambian continental margin offers improved understanding of the regional evolution of this complex 'passive' margin. Integrated with the regional geology, we can elude to the possible drivers behind the stratigraphic evolution (Figure 9). Further work constraining the vertical movements of the hinterland in Morocco (Charton, 2018) and in Mauritania (Gouiza et al., 2019; Lodhia, 2018) show that the 'passive' nature of the margin is punctuated by discrete uplift events (e.g. Leprêtre et al., 2015). The stratigraphic response in the sink records increased sediment input during these tectonic events as deduced from backstripping and subsidence analysis (Latil-Brun & Lucazeau, 1988). The Albian shelf-edge delta, recognised in this study, together with others along the margin (Figure 9; Mourlot, Calvès, et al., 2018; Mourlot, Roddaz, et al., 2018), represent the first major phase of siliciclastic sedimentation into the basin, potentially contributing to the demise of the Jurassic to Lower Cretaceous carbonate platform. Results from the analysis of neodymium isotope data delineate the segmented drainage of northwest Africa and the exhumation of Palaeozoic cover and Hercynian belts triggered by the opening of the Equatorial and South Atlantic was most likely the driver for delivering the siliciclastic influx during this period (Mourlot, Roddaz, et al., 2018). This is supported by new low-temperature thermochronology data recording exhumation of the Mauritanides between 180 and 100 Ma (Gouiza et al., 2019).

Prior to margin collapse, the Cenomanian–Turonian boundary records maximum transgression of the margin (Schlanger & Jenkyns, 1976), associated with a flattened peneplained topography (Flicoteaux, Latil-Brun, & Michaud, 1988). During this period, in the study area there are no collapse features or deposits observed, reflecting the quiescent geodynamic setting and high eustatic sea-level that resulted in a transgressed margin, where sedimentation is likely trapped in the onshore Senegal basin and/or drainage reorganisation shifts sediment input points laterally beyond the study area (Figure 1; Mourlot, Calvès, et al., 2018; Mourlot, Calvès, et al., 2018; Mourlot, Roddaz, et al., 2018). Further refinement of this model would be possible with access to well data located at the base of the carbonate escarpment, allowing for a more detailed stratigraphic interpretation and lithological control on these deposits.

Margin collapse at the scale and frequency observed through the Late Cretaceous is indicative of a significant change in accommodation (Playton et al., 2010). Covault, Fildani, Romans, and McHargue (2011) associate convex longitudinal canyon profiles (i.e. Figure 6c) with continental margin uplift and deformation. Several geodynamic events affecting the Central Atlantic are likely to manifest in vertical movements of the margin and eventual collapse, i.e. distal effects of the Santonian-aged early Alpine Orogeny compressional event, a shift in the pole of rotation of Atlantic spreading due to continental separation between Africa and South America (Guiraud & Bosworth, 1997; Labails, 2007) and similarly timed rifting episodes in Central Africa (Guiraud, 1998). Postulated Late Cretaceous volcanic uplift

of the Cape Verde islands and associated swell, *ca*. 500 km from the continental margin and study area, also affected the oceanic domain architecture (Figure 9; Casson et al., 2020). Regional uplift associated with this event may have created instability contributing to margin collapse. Tectonic stress accompanying these far-field events and linked to exhumation onshore was likely localised along the boundaries of the African plate (Gouiza et al., 2019). The base-of-slope in the study area directly overlies the continent–ocean boundary (Figure 1b). Further amplification of the base-level signal is expected due to relative changes in sea level (Haq, 2014), where, during lowstands, increased erosion within canyons is predicted due to canyons capturing more sediment input as depositional systems shift basinward (Pratson et al., 2007). However, canyon incision can also occur outside of lowstands (e.g. Fulthorpe et al., 2000). Linking the stratigraphic response to sea-level cyclicity would require a more detailed stratigraphic framework. Nevertheless, the timing of margin collapse is coeval with the relative first-order fall in sea level from the Coniacian to Maastrichtian, and expansion of drainage eastwards into the West African Craton (Figure 9; Haq, 2014; Mourlot, Roddaz, et al., 2018).

6 | CONCLUSIONS

The integration of seismic geomorphology with stratigraphic and lithological data from well data has allowed a quantitative evaluation of continental margin evolution, recording buried submarine canyons present on a RCU surface. This has significantly improved the understanding of the seascape evolution offshore The Gambia during the Cretaceous, developing a workflow and models applicable to the wider Central Atlantic and other continental margins worldwide. Thirteen submarine canyons are identified from the drainage model and geomorphological data extracted from these systems has been used to constrain two types of canyons, slope confined and shelf incised. The carbonate subcrop, which would have formed the seabed in the Aptian (the top Aptian surface), is interpreted to have been the main control on the location of knickpoints within these canyons and can be correlated with the sharp inflection in the slope profile. Through the Albian, a progradational shelf-edge delta delivered siliciclastic sediment with an extra-basinal provenance from hinterland drainage into the margin. It is likely subaqueous channel systems on the palaeo-shelf contributed to the early development of canyons due to erosion by downslope flowing turbidity currents, the depositional products forming a base-of-slope apron.

By utilising a semi-automated seismic interpretation and a geobody classification workflow, we are able to reconstruct the spatial-temporal evolution of mixed-system basin deposits linked to the submarine canyons and shelfal systems, providing insights into the early stages of canyon incision. Three main seismic facies are identified in the basin, debris-rich and debris-poor lobes, and MTDs. The integration of deposits linked to feeder canyon morphology reveals distinct types of canyons that originated both by gravity-flow and mass-wasting processes, with time-equivalent lateral variations along the margin.

Following establishment of the RCU, the margin began collapsing and canyonisation was initiated, intensifying during the Late Cretaceous. It is postulated this collapse was related to instability influenced by far-field tectonic stresses, with deformation localised on the margin of the African plate corresponding to the location of the platform margin study area. Locally derived sediment from the carbonate escarpment was incorporated and re-deposited in the basin by sediment mass transport events and sediment gravity flows. Volumetrically, shelf-incised canyons contributed on average an order of magnitude more sediment to the basin than slope-confined canyons. Large-km-scale blocks recognised in the seismic geomorphology of debris-rich lobes are interpreted to be carbonate detritus. The vast majority of canyon-derived sediment (97%) in the base-of-slope is observed to comprise of debris-rich lobes and hence, composed of locally derived material from the degradation of the pre-existing margin.

ACKNOWLEDGEMENTS

This study is part of the lead authors PhD project at the University of Manchester. We thank the sponsoring companies of the North Africa Research Group (NARG) for their continued financial and scientific support. We are grateful to TGS and Spectrum Geo for the provision of the seismic data, and we appreciate Felicia Winter's (TGS) comments on the preparation of figures and manuscript. We are thankful to Petrosen for permission to access the Senegal exploration wells. Alex Clarke (Cairn Energy) is thanked for his assistance with the seismic interpretation workflow. Andrew Newton (Queen's University Belfast) is thanked for the rose diagram spreadsheet tool. Early discussions of concepts with Keith Maynard (CGG Robertson) and Neil Mitchell (University of Manchester) helped with original concepts. Schlumberger (Petrel), Eliis (Paleoscan), ESRI (ArcMap; Arc Hydro) and Geoteric are thanked for academic licenses to the software used herein. Katherine Maier (National Institute of Water and Atmospheric Research), Zane Jobe (Colorado School of Mines), Andrea Fildani (Equinor) and Basin Research Editor-in-Chief, Atle Rotevatn, are thanked for their constructive reviews that improved the direction of this study.

DATA AVAILABILITY STATEMENT

The data that support the findings of this study are available from TGS. Restrictions apply to the availability of these data, which were used under license for this study. Data are available from the authors with the permission of TGS.

ORCID

Max Casson https://orcid.org/0000-0003-4241-3447
Gérôme Calvès https://orcid.org/0000-0003-3829-131X
Mads Huuse https://orcid.org/0000-0002-1766-4343
Ben Sayers https://orcid.org/0000-0002-9388-6781
Jonathan Redfern https://orcid.org/0000-0002-0536-1492

REFERENCES

Allen, P. A. (2008). From landscapes into geological history. *Nature*, *451*, 274–276.

Amblas, D., Canals, M., Urgeles, R., Lastras, G., Liquete, C., Hughes-Clarke, J. E., … Calafat, A. M. (2006). Morphogenetic mesoscale analysis of the northeastern Iberian margin, NW Mediterranean Basin. *Marine Geology*, *234*(1–4), 3–20.

Antobreh, A. A., & Krastel, S. (2006). Morphology, seismic characteristics and development of Cap Timiris Canyon, offshore Mauritania: A newly discovered canyon preserved-off a major arid climatic region. *Marine and Petroleum Geology*, *23*(1), 37–59.

Arthur, M. A., Dean, W. E., & Stow, D. A. V. (1984). Models for the deposition of Mesozoic-Cenozoic fine-grained organic-carbon-rich sediment in the deep sea. *Geological Society, London, Special Publications*, *15*(1), 527–560.

Bond, G. C., & Kominz, M. A. (1988). Evolution of thought on passive continental margins from the origin of geosynclinal theory (~ 1860) to the present. *Geological Society of America Bulletin*, *100*(12), 1909–1933.

Bond, G. C., Kominz, M. A., Steckler, M. S., Grotzinger, J. P., & Crevello, P. D. (1989). Role of thermal subsidence, flexure, and eustasy in the evolution of early Paleozoic passive-margin carbonate platforms. *Controls on Carbonate Platform and Basin Development: SEPM, Special Publication*, *44*, 39–61.

Bradley, D. C. (2008). Passive margins through earth history. *Earth-Science Reviews*, *91*(1–4), 1–26.

Braun, J., & Beaumont, C. (1989). A physical explanation of the relation between flank uplifts and the breakup unconformity at rifted continental margins. *Geology*, *17*(8), 760–764.

Brothers, D. S., Uri, S., Andrews, B. D., & Chaytor, J. D. (2013). Geomorphic characterization of the US Atlantic continental margin. *Marine Geology*, *338*, 46–63.

Brownfield, M. E., & Charpentier, R. R. (2003). *Assessment of the undiscovered oil and gas of the Senegal Province, Mauritania, Senegal, the Gambia, and Guinea-Bissau, Northwest Africa (25)*. Denver: US Department of the Interior, US Geological Survey.

Bull, S., Cartwright, J., & Huuse, M. (2009). A review of kinematic indicators from mass-transport complexes using 3D seismic data. *Marine and Petroleum Geology*, *26*(7), 1132–1151.

Burgess, P. M. (2001). Modelling carbonate sequence development without relative sea-level oscillations. *Geology*, *29*(12), 1127–1130.

Cartwright, J. A., & Lonergan, L. (1996). Volumetric contraction during the compaction of mudrocks: A mechanism for the development of regional-scale polygonal fault systems. *Basin Research*, *8*(2), 183–193.

Casson, M., Bulot, L. G., Jeremiah, J., & Redfern, J. (2020). Deep sea rock record exhumed on oceanic volcanic islands: The Cretaceous sediments of Maio, Cape Verde. *Gondwana Research*, *81*, 252–264.

Charton, R. J. G. (2018). *Phanerozoic vertical movements in Morocco*. Doctoral dissertation, TUDelft, Netherlands.

Chiarella, D., & Longhitano, S. G. (2012). Distinguishing depositional environments in shallow-water mixed, bio-siliciclastic deposits on the basis of the degree of heterolithic segregation (Gelasian, southern Italy). *Journal of Sedimentary Research*, *82*(12), 969–990.

Chiarella, D., Longhitano, S. G., & Tropeano, M. (2017). Types of mixing and heterogeneities in siliciclastic-carbonate sediments. *Marine and Petroleum Geology*, *88*, 617–627.

Clare, M., Chaytor, J., Dabson, O., Gamboa, D., Georgiopoulou, A., Eady, H., … León, R. (2019). A consistent global approach for the morphometric characterization of subaqueous landslides. *Geological Society, London, Special Publications*, *477*(1), 455–477.

Clayburn, J. (2017). *Realising the deepwater hydrocarbon potential of Senegal*. AAPG/SEG 2017 International Conference and Exhibition, London, England. Search and Discovery Article 70345.

Clift, P. D., Hodges, K., Heslop, D., Hannigan, R., Hoang, L. V., & Calvès, G. (2008). Greater Himalayan exhumation triggered by Early Miocene monsoon intensification. *Nature Geoscience*, *1*, 875–880.

Covault, J. A. (2011). Submarine fans and canyon-channel systems: A review of processes, products, and models. *Nature Education Knowledge*, *3*(10), 4.

Covault, J. A., Fildani, A., Romans, B. W., & McHargue, T. (2011). The natural range of submarine canyon-and-channel longitudinal profiles. *Geosphere*, *7*(2), 313–332.

Daly, R. A. (1936). Origin of submarine canyons. *American Journal of Science*, *186*, 401–420.

Davies, A. J., Roberts, J. M., & Hall-Spencer, J. (2007). Preserving deep-sea natural heritage: Emerging issues in offshore conservation and management. *Biological Conservation*, *138*(3–4), 299–312.

Davison, I. (2005). Central Atlantic margin basins of North West Africa: Geology and hydrocarbon potential (Morocco to Guinea). *Journal of African Earth Sciences*, *43*(1–3), 254–274.

Deptuck, M. E., Steffens, G. S., Barton, M., & Pirmez, C. (2003). Architecture and evolution of upper fan channel-belts on the Niger Delta slope and in the Arabian Sea. *Marine and Petroleum Geology*, *20*, 649–676.

Dingle, R. V., & Robson, S. (1985). Slumps, canyons and related features on the continental margin off East London, SE Africa (SW Indian Ocean). *Marine Geology*, *67*, 37–54.

Dugan, B., & Flemings, P. B. (2000). Overpressure and fluid flow in the New Jersey continental slope: Implications for slope failure and cold seeps. *Science*, *289*(5477), 288–291.

Farre, J. A., McGregor, B. A., Ryan, W. B., & Robb, J. M. (1983). Breaching the shelf break: Passage from youthful to mature phase in submarine canyon evolution. *SEPM Special Publication*, *33*, 25–39.

Fildani, A. (2017). Submarine canyons: A brief review looking forward. *Geology*, *45*(4), 383–384.

Fildani, A., Hubbard, S. M., Covault, J. A., Maier, K. L., Romans, B. W., Traer, M., & Rowland, J. C. (2013). Erosion at inception of deep-sea channels. *Marine and Petroleum Geology*, *41*, 48–61.

Fildani, A., Normark, W. R., Kostic, S., & Parker, G. (2006). Channel formation by flow stripping: Large-scale scour features along the Monterey East Channel and their relation to sediment waves. *Sedimentology*, *53*(6), 1265–1287.

Flicoteaux, R., Latil-Brun, M. V., & Michaud, L. (1988). Histoire de la subsidence post-rift du bassin côtier mauritano-sénégalo-guinéen. Relation avec l'amincissement crustal pendant la période jurassique à Crétacé inférieur. Comparaison avec l'évolution des marges péri-atlantiques au niveau de l'Atlantique Central et Equatorial (côte est des

USA, Sud-Sahara, Côte d'Ivoire et Plateau du Demerara). *Journal of African Earth Sciences (and the Middle East)*, *7*(2), 345–359.

Förster, R. (1978). Evidence for an open seaway between northern and southern proto-Atlantic in Albian times. *Nature*, *272*(5649), 158.

Fulthorpe, C. S., Austin, J. A. Jr, & Mountain, G. S. (2000). Morphology and distribution of Miocene slope incisions off New Jersey; are they diagnostic of sequence boundaries? *Geological Society of America Bulletin*, *112*, 817–828.

Galloway, W. E. (1975). Process framework for describing the morphologic and stratigraphic evolution of deltaic depositional systems. *Houston Geological Society*, 87–98.

Galloway, W. E. (1998). Siliciclastic slope and base-of-slope depositional systems: Component facies, stratigraphic architecture, and classification. *AAPG Bulletin*, *82*(4), 569–595.

George, A. D., Playford, P. E., & Powell, C. M. (1995). Platform-margin collapse during Famennian reef evolution, Canning Basin, Western Australia. *Geology*, *23*(8), 691–694.

Gouiza, M., Bertotti, G., Charton, R., Haimoudane, K., Dunkl, I., & Anczkiewicz, A. A. (2019). New evidence of anomalous' vertical movements along the Hinterland of the Atlantic NW African Margin. *Journal of Geophysical Research: Solid Earth*, *124*, 13333–13353. https://doi.org/10.1029/2019JB017914

Goumbo Lo, P., Dia, A., & Kampunzu, A. B. (1992). Cenozoic volcanism in Western Senegal and its relationship to the opening of the Central Atlantic Ocean. *Tectonophysics*, *209*, 281–291.

Granjeon, D., & Joseph, P. (1999). *Concepts and applications of a 3-D multiple lithology, diffusive model in stratigraphic modeling*. https://doi.org/10.2110/pec.99.62.0197

Guiraud, R. (1998). Mesozoic rifting and basin inversion along the northern African Tethyan margin: An overview. *Geological Society, London, Special Publications*, *132*(1), 217–229.

Guiraud, R., & Bosworth, W. (1997). Senonian basin inversion and rejuvenation of rifting in Africa and Arabia: Synthesis and implications to plate-scale tectonics. *Tectonophysics*, *282*(1–4), 39–82.

Haq, B. U. (2014). Cretaceous eustasy revisited. *Global and Planetary Change*, *113*, 44–58.

Harris, P. T., & Whiteway, T. (2011). Global distribution of large submarine canyons: Geomorphic differences between active and passive continental margins. *Marine Geology*, *285*(1–4), 69–86.

Hurd, G. S., Kerans, C., Fullmer, S., & Janson, X. (2016). Large-scale inflections in slope angle below the shelf break: A first order control on the stratigraphic architecture of carbonate slopes: Cutoff Formation, Guadalupe Mountains National Park, West Texas, USA. *Journal of Sedimentary Research*, *86*(4), 336–362.

Jansa, L. F. (1981). Mesozoic carbonate platforms and banks of the eastern North American margin. *Marine Geology*, *44*(1–2), 97–117.

Jobe, Z. R., Lowe, D. R., & Uchytil, S. J. (2011). Two fundamentally different types of submarine canyons along the continental margin of Equatorial Guinea. *Marine and Petroleum Geology*, *28*(3), 843–860.

Kelly, J., & Doust, H. (2016). Exploration for Late Cretaceous turbidites in the Equatorial African and northeast South American margins. *Netherlands Journal of Geosciences*, *95*(4), 393–403.

Kenter, J. A. M., & Campbell, A. E. (1991). Sedimentation on a Lower Jurassic carbonate platform flank: Geometry, sediment fabric and related depositional structures (Djebel Bou Dahar, High Atlas, Morocco). *Sedimentary Geology*, *72*, 1–34.

Klaus, A., & Taylor, B. (1991). Submarine canyon development in the Izu-Bonin forearc; a SeaMARC II and seismic survey of Aoga Shima Canyon. *Marine Geophysical Researches*, *13*, 105–130.

Kosmos Energy. (2017). *Investor Presentation – March 2017*. Dallas, Texas. Retrieved from https://www.kosmosenergy.com/

Labails, C. (2007). *La marge sud-marocaine et les premières phases d'ouverture de l'océan Atlantique Central*. Doctoral dissertation, Université de Bretagne Occidentale, France.

Labails, C., Olivet, J. L., Aslanian, D., & Roest, W. R. (2010). An alternative early opening scenario for the Central Atlantic Ocean. *Earth and Planetary Science Letters*, *297*(3–4), 355–368.

Lai, S. Y., Gerber, T. P., & Amblas, D. (2016). An experimental approach to submarine canyon evolution. *Geophysical Research Letters*, *43*(6), 2741–2747.

Lancelot, Y., Seibold, E., Cepek, P., Dean, W. E., Eremeev, V., Gardner, J. V., … Bukry, D. (1978a). Site 367: Cape Verde Basin. *Initial Reports of the Deep Sea Drilling Project*, *41*, 163–232.

Lancelot, Y., Seibold, E., Cepek, P., Dean, W. E., Eremeev, V., Gardner, J. V., … Bukry, D. (1978b). Site 368: Cape Verde Rise. *Initial Reports of the Deep Sea Drilling Project*, *41*, 233–326.

Land, L. A., Paull, C. K., & Spiess, F. N. (1999). Abyssal erosion and scarp retreat: Deep Tow observations of the Blake Escarpment and Blake Spur. *Marine Geology*, *160*(1–2), 63–83.

Latil-Brun, M. V. L., & Lucazeau, F. (1988). Subsidence, extension and thermal history of the West African margin in Senegal. *Earth and Planetary Science Letters*, *90*(2), 204–220.

Leprêtre, R., Missenard, Y., Barbarand, J., Gautheron, C., Saddiqi, O., & Pinna-Jamme, R. (2015). Postrift history of the eastern central Atlantic passive margin: Insights from the Saharan region of South Morocco. *Journal of Geophysical Research: Solid Earth*, *120*(6), 4645–4666.

Lodhia, B. H. (2018). *Dynamic subsidence, continental uplift and sedimentary deposition to West Africa's passive margin. (Doctoral dissertation)*. London, UK: Imperial College.

Lonergan, L., Jamin, N. H., Jackson, C. A. L., & Johnson, H. D. (2013). U-shaped slope gully systems and sediment waves on the passive margin of Gabon (West Africa). *Marine Geology*, *337*, 80–97.

Long, A., & Cameron, N. (2016). *Gravity and magnetic constraints and limitations in defining basin structure, offshore Senegal*. Petex 2016, Poster.

Maidment, D. R., & Morehouse, S. (2002). *Arc Hydro: GIS for water resources*. Redlands, CA: ESRI Inc.

Mann, P., Gahagan, L., & Gordon, M. B. (2003). Tectonic setting of the world's giant oil and gas fields. In M. T. Halbouty (Ed.). *Giant oil and gas fields of the decade 1990–1999: AAPG Memoir* 78, 15–105.

Martin, L., Effimoff, I., Medou, J., & Laughland, M. (2010). Hydrocarbon prospectivity of offshore Senegal-unlocking the door to a new deepwater petroleum province. Search and Discovery Article 10278.

Martinsen, O. J., Sømme, T. O., Thurmond, J. B., Helland-Hansen, W., & Lunt, I. (2010). Source-to-sink systems on passive margins: theory and practice with an example from the Norwegian continental margin. *Geological Society, London, Petroleum Geology Conference Series*, *7*(1), 913–920. https://doi.org/10.1144/0070913

McCave, I. N. (2017). Formation of sediment waves by turbidity currents and geostrophic flows: A discussion. *Marine Geology*, *390*, 89–93. https://doi.org/10.1016/j.margeo.2017.05.003

McGregor, B. (1985). Role of submarine canyons in shaping the rise between Lydonia and Oceanographer canyons, Georges Bank. *Marine Geology*, *62*, 277–293. https://doi.org/10.1016/0025-3227(85)90120-3

McHargue, T. R., Hodgson, D. M., & Shelef, E. (2019). Architectural diversity of submarine lobes. *EarthArXiv*. https://doi.org/10.31223/osf.io/cs8rp

McHugh, C. M., Ryan, W. B., & Schreiber, B. C. (1993). The role of diagenesis in exfoliation of submarine canyons. *AAPG Bulletin*, *77*(2), 145–172. https://doi.org/10.1306/BDFF8BB4-1718-11D7-8645000102C1865D

McIlreath, I. A., & James, N. P. (1978). Carbonate slopes. In R. G. Walker (Ed.), *Facies models: Geological Association of Canada, Geoscience Canada Series*, pp. 245–257.

McKenzie, D. (1978). Some remarks on the development of sedimentary basins. *Earth and Planetary Science Letters*, *40*(1), 25–32. https://doi.org/10.1016/0012-821X(78)90071-7

Meyer, F. O. (1989). Siliciclastic influence on Mesozoic platform development: Baltimore Canyon trough, western Atlantic. https://doi.org/10.2110/pec.89.44.0213

Miller, J. R. (1991). The influence of bedrock geology on knickpoint development and channel-bed degradation along downcutting streams in south-central Indiana. *The Journal of Geology*, *99*, 591–605. https://doi.org/10.1086/629519

Miller, K. G., Melillo, A. J., Mountain, G. S., Farre, J. A., & Wylie Poag, C. (1987). Middle to late Miocene canyon cutting on the New Jersey continental slope: biostratigraphic and seismic stratigraphic evidence. *Geology*, *15*(6), 509–512.

Mitchell, N. C. (2005). Interpreting long-profiles of canyons in the USA Atlantic continental slope. *Marine Geology*, *214*(1–3), 75–99.

Mitchell, N. C. (2006). Morphologies of knickpoints in submarine canyons. *Geological Society of America Bulletin*, *118*(5–6), 589–605.

Mitchum, R. M., & Vail, P. R. (1977). Seismic Stratigraphy and Global Changes of Sea Level: Part 7. *Seismic Stratigraphic Interpretation Procedure: Section 2. Application of Seismic Reflection Configuration to Stratigraphic Interpretation*.

Moscardelli, L., Ochoa, J., Lunt, I., & Zahm, L. (2019). Mixed siliciclastic–carbonate systems and their impact for the development of deep-water turbidites in continental margins: A case study from the Late Jurassic to Early Cretaceous Shelburne subbasin in offshore Nova Scotia. *AAPG Bulletin*, *103*(10), 2487–2520.

Moscardelli, L., & Wood, L. (2016). Morphometry of mass-transport deposits as a predictive tool. *Bulletin*, *128*(1–2), 47–80.

Moucha, R., Forte, A. M., Mitrovica, J. X., Rowley, D. B., Quéré, S., Simmons, N. A., & Grand, S. P. (2008). Dynamic topography and long-term sea-level variations: There is no such thing as a stable continental platform. *Earth and Planetary Science Letters*, *271*(1), 101–108.

Mourlot, Y., Calvès, G., Clift, P. D., Baby, G., Chaboureau, A. C., & Raisson, F. (2018). Seismic stratigraphy of Cretaceous eastern Central Atlantic Ocean: Basin evolution and palaeoceanographic implications. *Earth and Planetary Science Letters*, *499*, 107–121.

Mourlot, Y., Roddaz, M., Dera, G., Calvès, G., Kim, J. H., Chaboureau, A. C., … Raisson, F. (2018). Geochemical evidence for large-scale drainage reorganization in Northwest Africa during the Cretaceous. *Geochemistry, Geophysics, Geosystems*, *19*(5), 1690–1712.

Nelson, C. H., & Maldonado, A. (1988). Factors controlling depositional patterns of Ebro turbidite systems, Mediterranean Sea. *American Association of Petroleum Geologists Bulletin*, *72*, 698–716.

Nelson, C. H., Maldonado, A., Barber, J. H., & Alonso, B. (1991). Modern sand-rich and mud-rich siliciclastic aprons: Alternative base-of-slope turbidite systems to submarine fans. In Seismic facies and sedimentary processes of submarine fans and turbidite systems. In R. H. Dott, Jr. & R. H. Shaver (Eds.), *Modern and Ancient Geosynclinal Sedimentation*. Soc. Econ. Paleontol. Mineral., Spec. Publ., *19*, 56–68.

Normark, W. R. (1974). Submarine canyons and fan valleys Factors affecting growth patterns of deep-sea fans.

Normark, W. R., & Piper, D. W. (1969). Deep-sea fan-valleys, past and present. *Geological Society of America Bulletin*, *80*(9), 1859–1866. https://doi.org/10.1130/0016-7606(1969)80[1859:DFPAP]2.0.CO;2

Patruno, S., Hampson, G. J., & Jackson, C. A. (2015). Quantitative characterisation of deltaic and subaqueous clinoforms. *Earth-Science Reviews*, *142*, 79–119. https://doi.org/10.1016/j.earscirev.2015.01.004

Payros, A., & Pujalte, V. (2008). Calciclastic submarine fans: An integrated overview. *Earth-Science Reviews*, *86*(1–4), 203–246. https://doi.org/10.1016/j.earscirev.2007.09.001

Playton, T. E., Janson, X., Kerans, C., James, N. P., & Dalrymple, R. W. (2010). Carbonate slopes. *Facies Models*, *4*, 449–476.

Posamentier, H. W. (2005). Application of 3D seismic visualization techniques for seismic stratigraphy, seismic geomorphology and depositional systems analysis: examples from fluvial to deep-marine depositional environments. *Geological Society, London, Petroleum Geology Conference Series*, *6*(1), 1565–1576. https://doi.org/10.1144/0061565

Posamentier, H. W., & Kolla, V. (2003). Seismic geomorphology and stratigraphy of depositional elements in deep-water settings. *Journal of Sedimentary Research*, *73*(3), 367–388. https://doi.org/10.1306/111302730367

Pratson, L. F., & Coakley, B. J. (1996). A model for the headward erosion of submarine canyons induced by downslope-eroding sediment flows. *Geological Society of America Bulletin*, *108*(2), 225–234. https://doi.org/10.1130/0016-7606(1996)108<0225:AMFTHE>2.3.CO;2

Pratson, L. F., Nittrouer, C. A., Wiberg, P. L., Steckler, M. S., Swenson, J. B., Cacchione, D. A., … Mullenbach, B. L. (2007). Seascape evolution on clastic continental shelves and slopes. *Continental Margin Sedimentation: From Sediment Transport to Sequence Stratigraphy*, 339–380.

Pratson, L. F., & Ryan, W. B. (1996). Automated drainage extraction in mapping the Monterey submarine drainage system, California margin. *Marine Geophysical Researches*, *18*(6), 757–777. https://doi.org/10.1007/BF00313885

Prélat, A., Covault, J. A., Hodgson, D. M., Fildani, A., & Flint, S. S. (2010). Intrinsic controls on the range of volumes, morphologies, and dimensions of submarine lobes. *Sedimentary Geology*, *232*(1–2), 66–76.

Prélat, A., Pankhania, S. S., Jackson, C. A. L., & Hodgson, D. M. (2015). Slope gradient and lithology as controls on the initiation of submarine slope gullies; insights from the North Carnarvon Basin, offshore NW Australia. *Sedimentary Geology*, *329*, 12–17.

Principaud, M., Mulder, T., Gillet, H., & Borgomano, J. (2015). Large-scale carbonate submarine mass-wasting along the northwestern slope of the Great Bahama Bank (Bahamas): Morphology, architecture, and mechanisms. *Sedimentary Geology*, *317*, 27–42.

Puga-Bernabéu, Á., Webster, J. M., Beaman, R. J., & Guilbaud, V. (2011). Morphology and controls on the evolution of a mixed carbonate–siliciclastic submarine canyon system, Great Barrier Reef margin, north-eastern Australia. *Marine Geology*, *289*(1–4), 100–116.

Reuber, K. R., Pindell, J., & Horn, B. W. (2016). Demerara Rise, offshore Suriname: Magma-rich segment of the Central Atlantic Ocean, and conjugate to the Bahamas hot spot. *Interpretation*, *4*(2), 141–155.

Schlanger, S. O., & Jenkyns, H. C. (1976). Cretaceous oceanic anoxic events: Causes and consequences. *Geologie En Mijnbouw*, *55*(3–4).

Shepard, F. P. (1934). Canyons off the New England coast. *American Journal of Science*, *157*, 24–36.

Shumaker, L. E., Jobe, Z. R., & Graham, S. A. (2017). Evolution of submarine gullies on a prograding slope: Insights from 3D seismic reflection data. *Marine Geology*, *393*, 35–46.

Sømme, T., Helland-Hansen, W., Martinsen, O. J., & Thurmond, J. B. (2009). Relationships between morphological and sedimentological parameters in source-to-sink systems: A basis for predicting semi-quantitative characteristics in subsurface systems. *Basin Research*, *21*, 361–387.

Steckler, M. S., Watts, A. B., & Thorne, J. A. (1988). Subsidence and basin modeling at the US Atlantic passive margin. *The Geology of North America*, *2*, 399–416.

Steel, R. J., Porebski, S. J., Plink-Bjorklund, P., Mellere, D., & Schellpeper, M. (2003). Shelf-edge delta types and their sequence-stratigraphic relationships. *Shelf Margin Deltas and Linked down Slope Petroleum Systems*, 205–230.

Stevenson, C. J., Jackson, C. A. L., Hodgson, D. M., Hubbard, S. M., & Eggenhuisen, J. T. (2015). Deep-water sediment bypass. *Journal of Sedimentary Research*, *85*(9), 1058–1081. https://doi.org/10.2110/jsr.2015.63

Sylvester, Z., Deptuck, M. E., Prather, B. E., Pirmez, C., O'Byrne, C., Mohrig, D., … Wynn, R. B. (2012). Seismic stratigraphy of a shelf-edge delta and linked submarine channels in the northeastern Gulf of Mexico. *Application of the Principles of Seismic Geomorphology to Continental-Slope and Base-of-Slope Systems: Case Studies from Seafloor and Near-Seafloor Analogues: SEPM, Special Publication*, *99*, 31–59.

Talling, P. J. (2013). Hybrid submarine flows comprising turbidity current and cohesive debris flow: Deposits, theoretical and experimental analyses, and generalized models. *Geosphere*, *9*(3), 460–488. https://doi.org/10.1130/GES00793.1

Tari, G., Molnar, J., & Ashton, P. (2003). Examples of salt tectonics from West Africa: A comparative approach. *Geological Society, London, Special Publications*, *207*(1), 85–104. https://doi.org/10.1144/GSL.SP.2003.207.5

Twichell, D. C., & Roberts, D. G. (1982). Morphology, distribution, and development of submarine canyons on the United States Atlantic continental slope between Hudson and Baltimore Canyons. *Geology*, *10*(8), 408–412.

Uchupi, E., & Emery, K. O. (1991). Pangaean divergent margins: Historical perspective. *Marine Geology*, *102*(1–4), 1–28. https://doi.org/10.1016/0025-3227(91)90003-M

Uchupi, E., Emery, K. O., Bowin, C. O., & Phillips, J. D. (1976). Continental margin off western Africa: Senegal to Portugal. *AAPG Bulletin*, *60*(5), 809–878. https://doi.org/10.1306/C1EA35BE-16C9-11D7-8645000102C1865D

Wegener, A. (1912). The origin of continents. *Petermanns Geographische Mitteilungen*, *58*, 185–309.

Wood, L. J. (2007). Quantitative seismic geomorphology of Pliocene and Miocene fluvial systems in the northern Gulf of Mexico, USA. *Journal of Sedimentary Research*, *77*(9), 713–730. https://doi.org/10.2110/jsr.2007.068

Wynn, R. B., Masson, D. G., Stow, D. A., & Weaver, P. P. (2000a). The Northwest African slope apron: A modern analogue for deep-water systems with complex seafloor topography. *Marine and Petroleum Geology*, *17*(2), 253–265. https://doi.org/10.1016/S0264-8172(99)00014-8

Wynn, R. B., Masson, D. G., Stow, D. A. V., & Weaver, P. P. E. (2000b). Turbidity current sediment waves on the submarine slopes of the western Canary Islands. *Marine Geology*, *163*, 185–198. https://doi.org/10.1016/S0025-3227(99)00101-2

Wynn, R. B., & Stow, D. A. (2002). Classification and characterisation of deep-water sediment waves. *Marine Geology*, *192*(1–3), 7–22. https://doi.org/10.1016/S0025-3227(02)00547-9

How to cite this article: Casson M, Calvès G, Huuse M, Sayers B, Redfern J. Cretaceous continental margin evolution revealed using quantitative seismic geomorphology, offshore northwest Africa. *Basin Res*. 2020;00:1–25. https://doi.org/10.1111/bre.12455